AD-A270 436

(1)

WL-TR-93-7032

Laser Imaging Radar System

Steven P. Yun
Robert A. Olson

Schwartz Electro-Optics, Inc.
3404 N. Orange Blossom Trail
Orlando FL 32804

SEPTEMBER 1993

FINAL REPORT FOR PERIOD AUGUST 1989 - APRIL 1993

Approved for public release; distribution is unlimited.

DTIC
ELECTE
OCT 12 1993
S B D

WRIGHT LABORATORY, ARMAMENT DIRECTORATE
Air Force Materiel Command ▮ United States Air Force ▮ Eglin Air Force Base

93-23972

NOTICE

When Government drawings, specifications, or other data are used for any purpose other than in connection with a definitely Government-related procurement, the United States Government incurs no responsibility or any obligation whatsoever. The fact that the Government may have formulated or in any way supplied the said drawings, specifications, or other data, is not to be regarded by implication, or otherwise as in any manner construed, as licensing the holder, or any other person or corporation; or as conveying any rights or permission to manufacture, use, or sell any patented invention that may in any way be related thereto.

This technical report has been reviewed and is approved for publication.

The Public Affairs Office has reviewed this report, and it is releasable to the National Technical Information Service (NTIS), where it will be available to the general public, including foreign nationals.

FOR THE COMMANDER

MICHAEL L. DE LORENZO, Lt Col, USAF
Chief, Advanced Guidance Division

Even though this report may contain special release rights held by the controlling office, please do not request copies from the Wright Laboratory, Armament Directorate. If you qualify as a recipient, release approval will be obtained from the originating activity by DTIC. Address your request for additional copies to:

Defense Technical Information Center
Cameron Station
Alexandria VA 22304-6145

If your address has changed, if you wish to be removed from our mailing list, or if your organization no longer employs the addressee, please notify WL/MNGS, Eglin AFB FL 32542-6810, to help us maintain a current mailing list.

Do not return copies of this report unless contractual obligations or notice on a specific document requires that it be returned.

REPORT DOCUMENTATION PAGE

Form Approved
OMB No. 0704-0188

Public reporting burden for this collection of information is estimated to average 1 hour per response, including the time for reviewing instructions, searching existing data sources, gathering and maintaining the data needed, and completing and reviewing the collection of information. Send comments regarding this burden estimate or any other aspect of this collection of information, including suggestions for reducing this burden, to Washington Headquarters Services, Directorate for Information Operations and Reports, 1215 Jefferson Davis Highway, Suite 1204, Arlington, VA 22202-4302, and to the Office of Management and Budget, Paperwork Reduction Project (0704-0188), Washington, DC 20503

1. AGENCY USE ONLY *(Leave blank)*

2. REPORT DATE
September 1993

3. REPORT TYPE AND DATES COVERED
Final, August 1989 - April 1993

4. TITLE AND SUBTITLE
Laser Imaging Radar System

5. FUNDING NUMBERS
C: F08635-90-C-0050
PE: 65502F
PR: 3005
TA: 80
WU: 31

6. AUTHOR(S)
Steven P. Yun and Robert A. Olson

7. PERFORMING ORGANIZATION NAME(S) AND ADDRESS(ES)
Schwartz Electro-Optics, Inc.
3404 N. Orange Blossom Trail
Orlando FL 32804

8. PERFORMING ORGANIZATION REPORT NUMBER

9. SPONSORING/MONITORING AGENCY NAME(S) AND ADDRESS(ES)
Wright Laboratory, Armament Directorate
Advanced Guidance Division
Sensor Technology Branch (WL/MNGS)
Eglin AFB FL 32542-6810

10. SPONSORING/MONITORING AGENCY REPORT NUMBER
WL-TR-93-7032

11. SUPPLEMENTARY NOTES

12a. DISTRIBUTION/AVAILABILITY STATEMENT
Approved for public release; distribution is unlimited.

12b. DISTRIBUTION CODE
A

13. ABSTRACT *(Maximum 200 words)*
The simplicity, compactness, and reasonable cost of direct detection diode-laser range finders provide incentive for their use in laser imaging radar systems (LIRS). Efforts have been made to increase range performance of a diode-laser range finder by means of narrow bandwidth operation. This involved narrowing the line width of the diode laser via a narrow bandwidth filter in an external cavity so that it was compatible with a 5 Å receiver filter. The narrow bandwidth of the receiver filter limited the amount of solar background radiation incident upon the receiver, thereby increasing the signal-to-noise ratio and thus maximizing the range capability. The study comprised the development and testing of a line-narrowed single-element diode-laser range finder, an analysis of multi-element diode-laser geometries, and an experimental evaluation of diode-laser collimation by means of a cylindrical microlens.

14. SUBJECT TERMS
External Cavity, Line-Narrowed Diode-Laser Range Finder

15. NUMBER OF PAGES
63

16. PRICE CODE

17. SECURITY CLASSIFICATION OF REPORT
UNCLASSIFIED

18. SECURITY CLASSIFICATION OF THIS PAGE
UNCLASSIFIED

19. SECURITY CLASSIFICATION OF ABSTRACT
UNCLASSIFIED

20. LIMITATION OF ABSTRACT
UL

PREFACE

This final report was prepared by Schwartz Electro-Opitcs, Inc., 3404 N. Orange Blossom Trail, Orlando FL 32804, under contract F08635-90-C-0050 with WL/MN, Eglin Air Force Base, Fl 32542-6810. Capt John Dargan managed the program for the Armament Directorate. The program was conducted during the period from August 1989 to April 1993.

TABLE OF CONTENTS

Section	Title	Page
I	INTRODUCTION	1
II	SUMMARY OF PHASE I RESULTS	2
III	PHASE II TECHNICAL RESULTS	3
	1. SINGLE-ELEMENT LASER SOURCE DEVELOPMENT	3
	a. Antireflection-Coated Diode Lasers	3
	b. Narrow-Bandpass Filter	9
	c. External-Cavity Diode Laser	18
	2. LINE-NARROWED DIODE-LASER RANGE FINDER	32
	a. System Design	32
	b. System Tests	35
	3. MULTI-ELEMENT LASER SOURCE DEVELOPMENT	40
	4. DIODE-LASER COLLIMATION VIA CYLINDRICAL MICROLENS	44
IV	CONCLUSION	50
V	REFERENCES	52

Accession For
NTIS GRA&I ☑
DTIC TAB ☐
Unannounced ☐
Justification
By
Distribution/
Availability Codes
Dist | Avail and/or Special
A-1

LIST OF FIGURES

Figure	Title	Page
1	SiO_x refractive index as a function of O_2 partial pressure	4
2	GRINSCH laser power as a function of SiO_x coating thickness	6
3	GRINSCH laser forward voltage as a function of SiO_x coating thickness	7
4	Spectra of the AR-coated diode laser device for coating run #1	8
5	Gain versus bias current of the AR-coated diode laser device for coating run #1	9
6	Filter transmission curve at 830 nm	11
7	Filter transmission curve at 830 nm	12
8	Filter transmission curve at 830 nm	13
9	Filter transmission curve at 820 nm	14
10	Filter transmission curve at 820 nm	15
11	Filter transmission curve at 910 nm	16
12	Filter transmission curve at 910 nm	17
13	Original line narrowing optical setup	19
14	Output power curve for collimated laser diode	21
15	Output power curve for output coupler misaligned (curve a), and output coupler aligned (curve b) with external cavity	21
16	Output power curve for the external cavity with an intra-cavity filter	22
17	Spectra characteristics of the collimated AR-coated device	22
18	Spectra characteristics of the AR-coated device in an external cavity	23
19	Spectra characteristics of the AR-coated device in an external cavity with an intra-cavity bandpass filter	23
20	Measured pulse width with 2" filter	24
21	Spectral width without filter	25
22	Spectral width with feedback	25
23	Spectral width intra-cavity filter & feedback	26
24	Spectral bandwidth of the CVD-62 versus output coupler transmission	29
25	Modified line-narrowing optical setup	31

LIST OF FIGURES (cont.)

Figure	Title	Page
26	Line-narrowed range finder	33
27	Optical receiver block diagram	33
28	Analog range counter block diagram	35
29	Computer-simulated data for the line-narrowed range finder	37
30	Conventional range finder	39
31	Computer-simulated data for the line-narrowed range finder	39
32	Schematic illustration of resonator misaligned with one collimation lens and multiple diode elements	41
33	Multi-element line-narrowed diode-laser resonator geometry employing GRIN lens collimators	41
34	Mounting configuration for three 18-mm aperture collimating lenses	43
35	Microlens positioning setup	45
36	Cylindrical microlens collimator	46
37	Microlens-collimated beam intensity contour and profile plots	47
38	Beam intensity contour and profile plots after epoxy cure	48
39	Beam intensity contour and profile plots after disconnecting lens positioner	49

LIST OF TABLES

Table	Title	Page
1	Diode laser power and bandwidth data	24
2	Peak power vs. supply voltage with the output coupler misaligned and optimally aligned for feedback	27
3	Test results with various output couplers	28
4	Output power and spectral bandwidth at various locations	31
5	Test results from line-narrowed system	36
6	Test results from conventional system	38

LIST OF ABBREVIATIONS ACRONYMS AND SYMBOLS

A	ampere
APD	avalanche photodiode detector
$A/\sqrt{Hz}$	ampere per root hertz
AR	antireflection
cm	centimeter
CW	continuous wave
EBAC	Ensign Bickford Aerospace Company
F	Fahrenheit
ft	foot
FWHM	Full wave half maximum
f/0.9	F/number 0.9
GRINSCH	Graded Index Single Confinement Heterostructure
GRIN	graded-index
I/O	input/output
kHz	kilohertz
kΩ	kilohms
LDL	Laser Diode Labs
LIRS	Laser Imaging Radar System
m	meter
mils	1/1000 inch
mm	millimeter
MOCVD	metal organic chemical vapor deposition
MOSFET	metal-oxide-semiconductor field-effect transistor
mrad	milliradian
N A	numerical aperture
nm	nanometer
ns	nanosecond

LIST OF ABBREVIATIONS ACRONYMS AND SYMBOLS (cont.)

ns/Div	nanosecond per division
$pA/\sqrt{Hz}$	picoampere per root hertz
R	reflective
rms	root mean square
SDL	Spectra Diodes Labs
SEO	Schwartz Electro-Optics
T	transmission
T_{pk}	peak transmission
Typ.	typical
V	volt
W	Watts
W/Å	watts per angstrom
°C	degrees Celsius
λ_c	center wavelength
$\Delta\lambda_{FWHM}$	change in wavelength at full wave half maximum
μs	microsecond
ϕ_{pk}	peak optical power

SECTION I
INTRODUCTION

The simplicity, compactness, and reasonable cost of direct-detection diode-laser range finders provide incentive for their use in laser imaging radar systems (LIRS) for airborne target-detection applications. Unfortunately, the maximum range of diode-laser range finders is limited by the low (order of 10 W) peak output powers and broad (order of 5 nm) linewidth characteristic of diode lasers, as compared to the multi-kilowatt peak powers and Angstrom linewidths of solid-state lasers.

This report describes the results of an effort to increase the range performance of a diode-laser range finder by means of narrow-bandwidth operation. This involved narrowing the linewidth of the diode laser via a narrow-band filter in an external cavity so that it was compatible with a 5 Å receiver filter. The narrow bandwidth of the receiver filter limited the amount of solar background radiation incident upon the receiver, thereby increasing the signal-to-noise ratio and thus the maximum range capability.

A summary of the results of the Phase I LIRS effort is given in Section II. The results of the Phase II study are presented in Section III. The study comprised the development and testing of a line-narrowed single-element diode-laser range finder, an analysis of multi-element diode-laser geometries, and an experimental evaluation of diode-laser collimation by means of a cylindrical microlens. Conclusions are given in Section IV.

SECTION II
SUMMARY OF PHASE I RESULTS

The Phase I LIRS effort comprised 1) a system analysis which compared the performance of a conventional system with that of a line-narrowed system, 2) a line-narrowed diode laser proof-of-principle experiment, and 3) range-image data generated by a conventional LIRS system.

A system analysis was carried out for conventional and line-narrowed laser imaging radar systems employing pulsed-diode-laser transmitters and avalanche-photodiode direct detection receivers equipped with optical bandpass filters. The conventional system was based upon a 50 W peak-power diode laser ($\simeq$ 5 nm linewidth) and a 40 nm receiver filter. The line-narrowed system was based upon a 30 W peak-power line-narrowed diode laser ($\simeq$ 1 nm linewidth) and a matching 1 nm receiver filter. The analysis showed, for the same conditions of target/background reflectance, atmospheric attenuation, probability of detection and false alarm, and solar spectral irradiance, that the maximum range for the conventional system was 1000 ft, whereas that for the line-narrowed system was 1600 ft.

The line-narrowing proof-of-principle experiment employed a diode-laser chip with a high reflectance coating on the rear facet and an AR coating on the front facet. The emission from the chip was collimated by an 8 mm focal length multi-element lens (0.5 N.A.). A flat, partially reflecting mirror provided the feedback required to obtain laser oscillation. A 0.9 nm bandpass filter within the resonator was used to achieve line narrowing. A laser linewidth of 0.8 nm (FWHM) was measured with a 0.64 m Czerny-Turner spectrometer with a 600 groove/mm grating operating in second order.

A false-color range image of an M-48 tank at a range of 300 ft obtained with a conventional LIRS was presented. The 0.42 ft range resolution of the false-color (32 colors) image resulted in excellent discrimination between target and background. A range profile of the image suitable for target identification was also presented.

SECTION III
PHASE II TECHNICAL RESULTS

1. SINGLE-ELEMENT LASER SOURCE DEVELOPMENT

a. Antireflection-Coated Diode Lasers

In order to find a diode laser manufacturer to develop an antireflection (AR)-coated diode laser, two manufacturers -- Spectra Diodes Lab (SDL) and Laser Diode Labs (LDL) -- were approached to develop low facet reflectivity (< 0.1%) laser diodes. SDL does not have the capability to do AR coating with such low reflectivity and was not interested in developing the technology within the required budget and schedule. After discussing various techniques that would be used to achieve a 0.1% AR coating, LDL decided that they were interested in developing this technique.

Two major problems in the AR coating development were encountered and solved. The first problem was the difficulty experienced in obtaining uniform and reproducible SiO_x deposition when using the conventional e-beam impingement technique with SiO chunks. The solution to this problem was to evaporate pure Si under a controlled partial pressure of O_2. The Si melt geometry provides a uniform deposition profile, and the O_2 partial pressure controls the SiO_x composition and hence refractive index (see Figure 1). The second problem, related to the two monitoring techniques chosen, was that the large-area diode laser device was unstable when operated CW (note: this device is normally operated in the pulsed mode) in the vacuum coating chamber because of thermal degradation. The solution to this problem was to use a Graded Index Single Confinement Heterostructure (GRINSCH) quantum well diode laser that was developed at Laser Diode, Inc. as the CW monitor device. At the time, only 880 nm GRINSCH devices were available, and the wavelength of the monitor device must match that of the devices to be AR-coated. LDL proceeded with the AR coating development at 880 nm while a wafer of 830 nm GRINSCH devices was being processed.

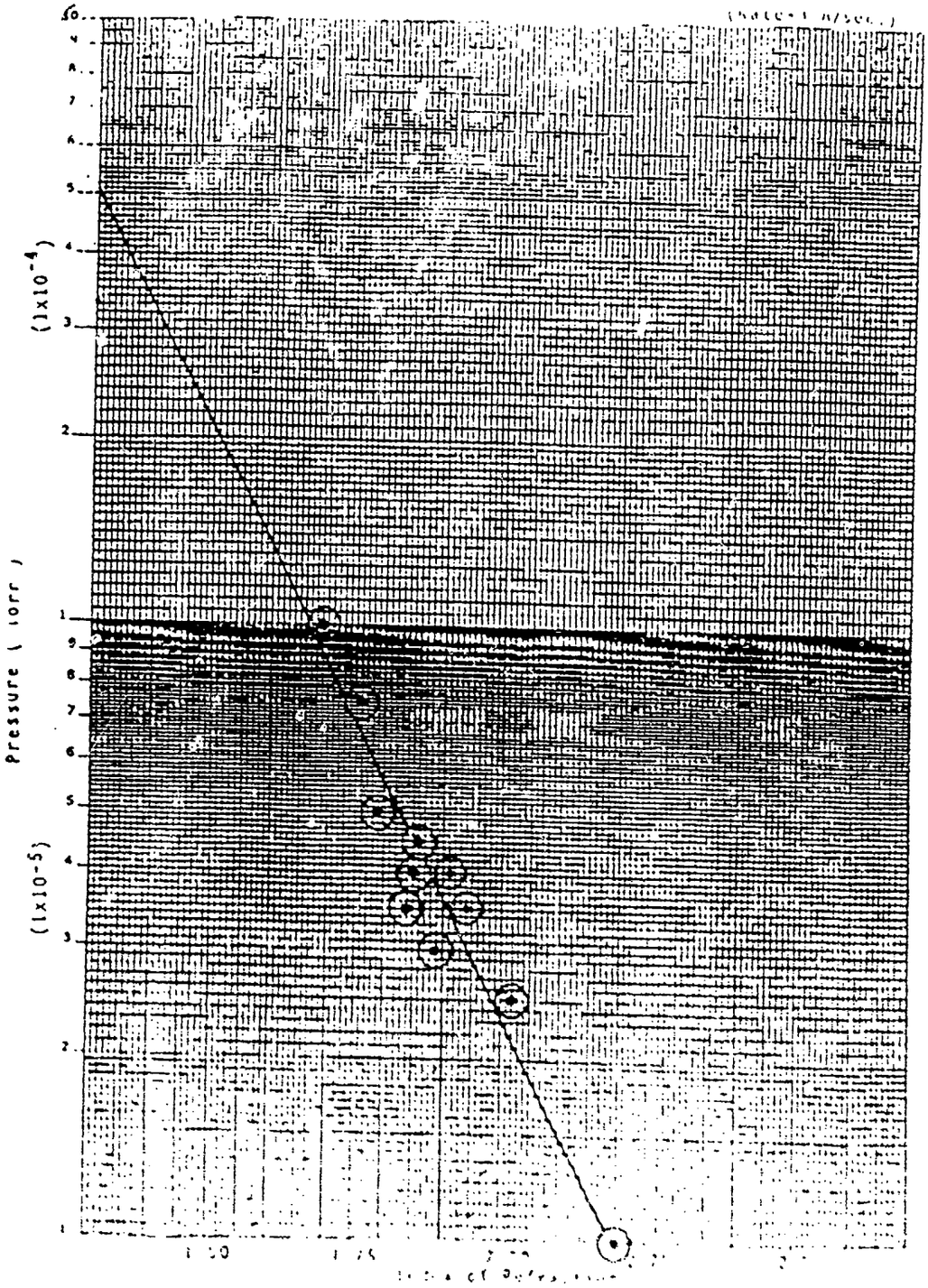

Figure 1 SiO_x refractive index as a function of O_2 partial pressure

LDL compared the two different AR coating monitoring techniques, laser power from the rear facet (see Figure 2) and device forward voltage (see Figure 3), as a function of coating thickness (measured with a crystal mass monitor). The laser power should decrease as the optimum coating thickness is approached while the forward voltage increases to a peak [1]. The data shown in Figure 2 and 3 are for a GRINSCH monitor device. The forward-voltage technique consistently provided a well-defined peak at optimum coating thickness, while the power monitor provided an ill-defined plateau. The required quarter-wave coating at 880 nm should be 115.8 nm thick SiO_x for 1.9 refractive index in accordance with the data of Figure 5. The forward-voltage monitoring technique was chosen as the technique to be used to monitor the 830 nm AR coating.

The first AR-coated diode lasers (front facet AR, rear facet 95% R) from LDL were evaluated at SEO, Concord, Massachusetts. The estimated residual reflectivity of the AR coated facet was approximately 3.5×10^{-3}. The residual facet reflectivity was determined from the modulation of the device emission spectrum [2] by Fabry-Perot fringes resulting from the facet reflections. The modulated spectra must be obtained under CW bias to prevent the frequency chirping associated with pulsed operation from obscuring the modulation fringes.

Time-averaged spectra taken with a 0.64 m grating spectrometer (0.01 nm resolution) are shown, as a function of CW bias current, in Figure 4. Following the analysis of Kaminow et al [2], we can define a modulation index (m)

$$m = \frac{P_{max} - P_{min}}{P_{max} + P_{min}} \qquad (1)$$

where P_{max} and P_{min} refer to the extreme of the fringe modulation at the peak of the emission spectrum. The round trip gain ($|a|$) is related to the modulation index by

$$m = \frac{2|a|}{1+|a|^2} \qquad (2)$$

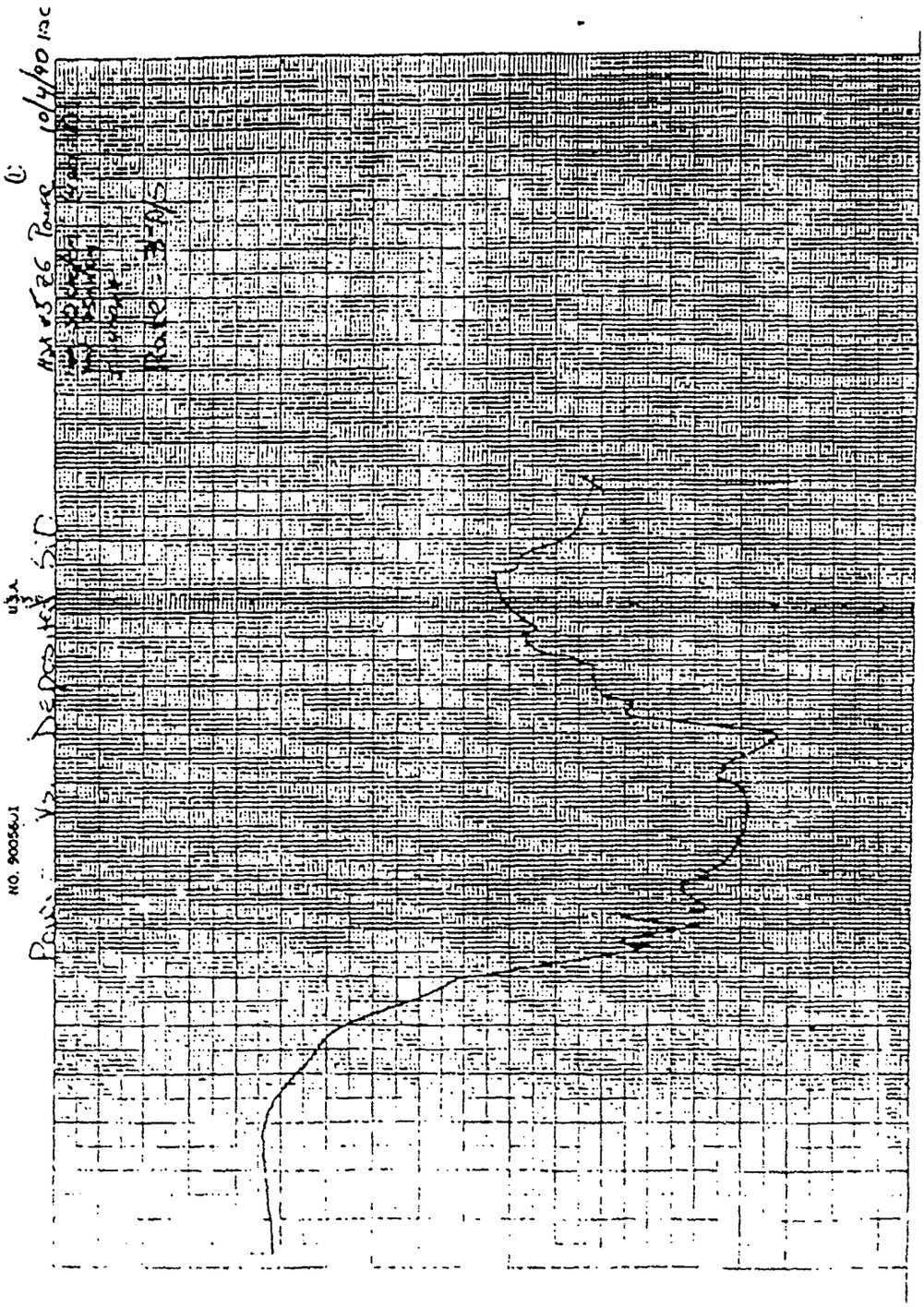

Figure 2 GRINSCH laser power as a function of SiO_x coating thickness

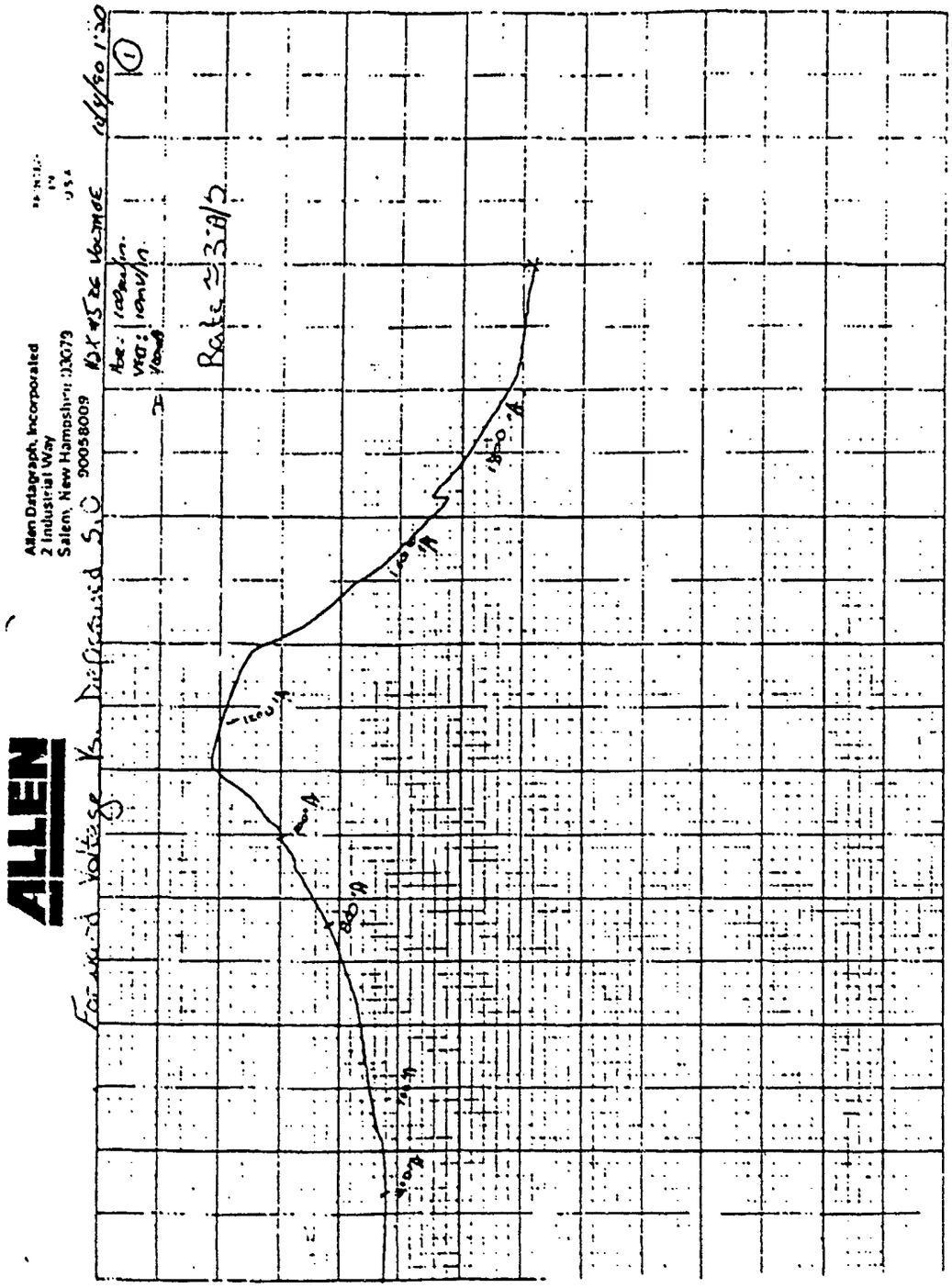

Figure 3. GRINSCH laser forward voltage as a function of SiO_x coating thickness

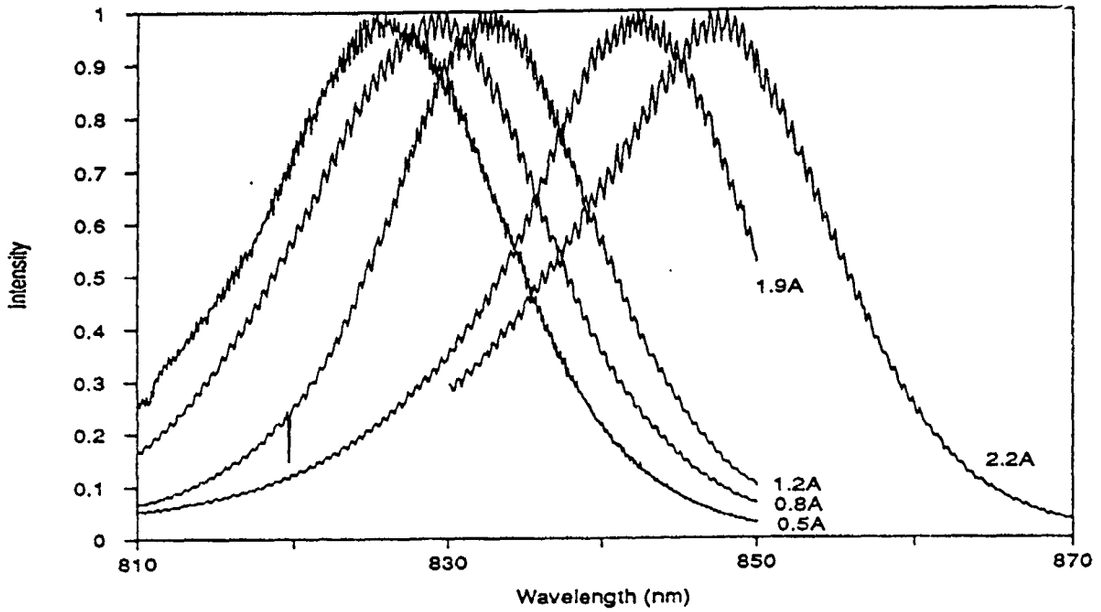

Figure 4. Spectra of the AR-coated diode laser device for coating run #1

The round trip gain can be defined by

$$\ln|a| = (\gamma L)\frac{I}{I_t} - \left(\gamma L - \ln\frac{\sqrt{R_1 R_2}}{R_l}\right) \qquad (3)$$

where I is the diode laser drive current, I_t is the threshold current of the diode laser, γ is the power gain coefficient at $I=I_t$, L is the length of the diode chip, R_1 is the AR-coated output facet reflectance, R_2 is the back facet reflectance, and R_l is the nominal output facet reflectance. Equation 3 may be used to fit the gain data derived from the spectral modulation well below laser threshold in the absence of gain saturation. Figure 5 shows the gain as a function of bias current. Unfortunately, there was insufficient data in the linear region to provide an unambiguous fit to Equation (3). However, the residual reflectivity can be determined from the coating parameters and its consistency with the data in Figure 5 evaluated.

A silicon monitor placed near the laser material in the coating chamber was analyzed by ellipsometry to determine the refractive index (1.87) and thickness (105 nm) of the SiO_x layer. If an ideal index match (i.e., $n_{device} = n^2_{coating}$) at the emission wavelength of 830 nm is assumed, the calculated residual reflectivity is 3.5×10^{-3}. The dashed line on Figure 5 represents Equation (3) for the residual reflectivity of 3.5×10^{-3} and shows qualitative agreement.

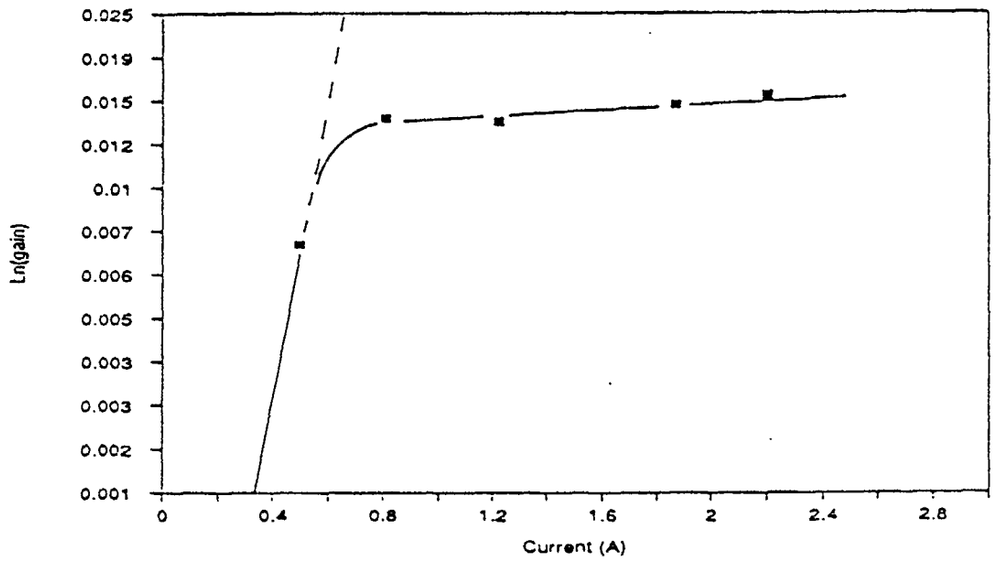

Figure 5. Gain versus bias current of the AR-coated diode laser device for coating run #1

b. Narrow-Bandpass Filter

After lengthy discussions with several bandpass filter manufacturers, orders for a single sample device were placed with two vendors, Spectro-film and Andover Corp. Both vendors were asked to produce a 0.5 nm FWHM bandpass filter at 830 nm with maximum transmission as the primary goal. Using a two-cavity filter design with no optical blocking elements, the vendors were able to fabricate 0.5 nm FWHM bandpass filters, Andover's filter had transmission of 86%, as shown in Figure 6, while Spectral-film's filter had transmission of 42%.

Based upon the performance of the initial bandpass filter purchase, an order was placed with Andover Corp. to investigate the reproducibility of the bandpass filters. Several small orders were placed, instead of one large one, in order to develop a data base on filter bandwidth and peak transmission variations at wave lengths of 830 nm, 820, nm and 910 nm. In discussions on filter transmission, Andover Corp. indicated that the 86% transmission already obtained was probably the best that could be expected due to absorption in the dielectric materials used for the filter cavities.

The 0.5 nm FWHM bandpass filters at 830 nm had peak transmissions of 87% and 74%. The test data for the filters at 830 nm are shown in Figure 7 and 8. The lower transmission filter has two transmission peaks that are shifted and thereby block one another. This reduces the peak transmission and is indicative of a mismatch between the two Fabry-Perot stacks used for the filter. Andover Corp. stated that typically 20% of all coating runs result in mismatch stacks for such narrow bandpass filter.

The 0.5 nm FWHM bandpass filters at 820 nm had peak transmissions of 75% and 81%. The test data for the filters at 820 nm are shown in Figure 9 and 10. The 0.5 nm FWHM bandpass filters at 910 nm had peak transmissions of 61% and 65%. The test data for the filters at 910 nm are shown in Figure 11 and 12 According to Andover Corp., the filters at 910 nm had low transmission because of the absorption of the dielectric materials at that center wavelength.

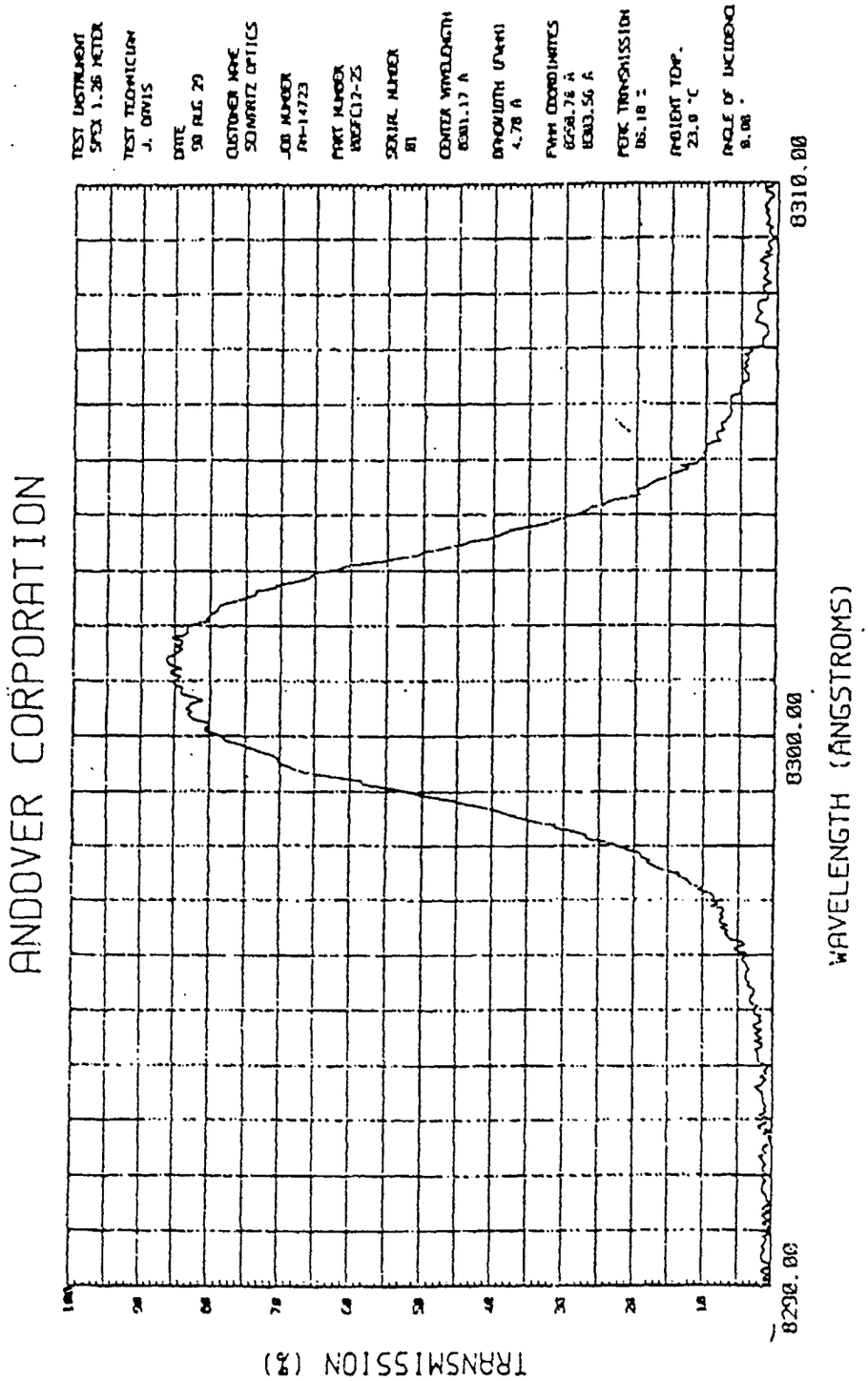

Figure 6. Filter transmission curve at 830 nm

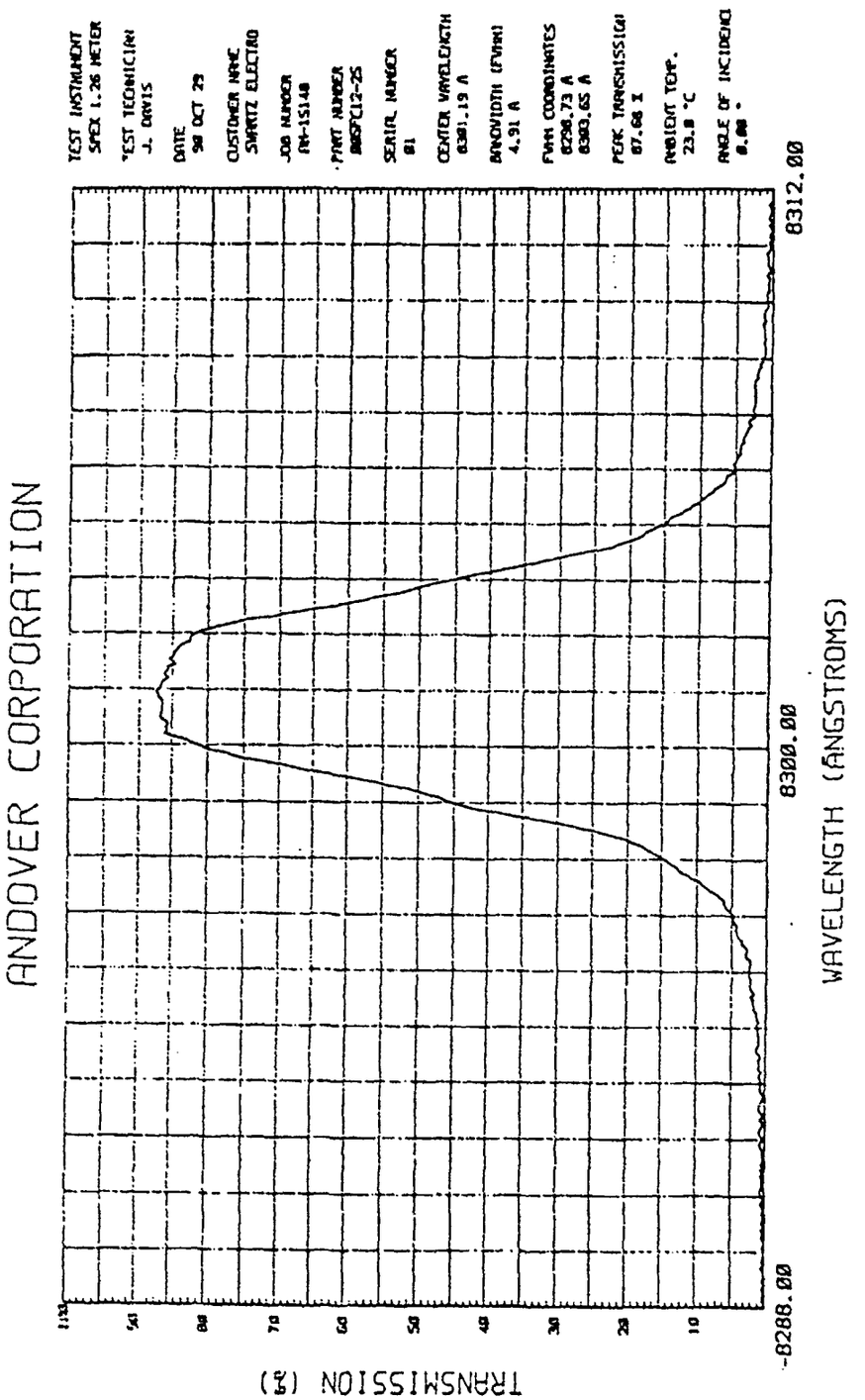

Figure 7. Filter transmission curve at 830 nm

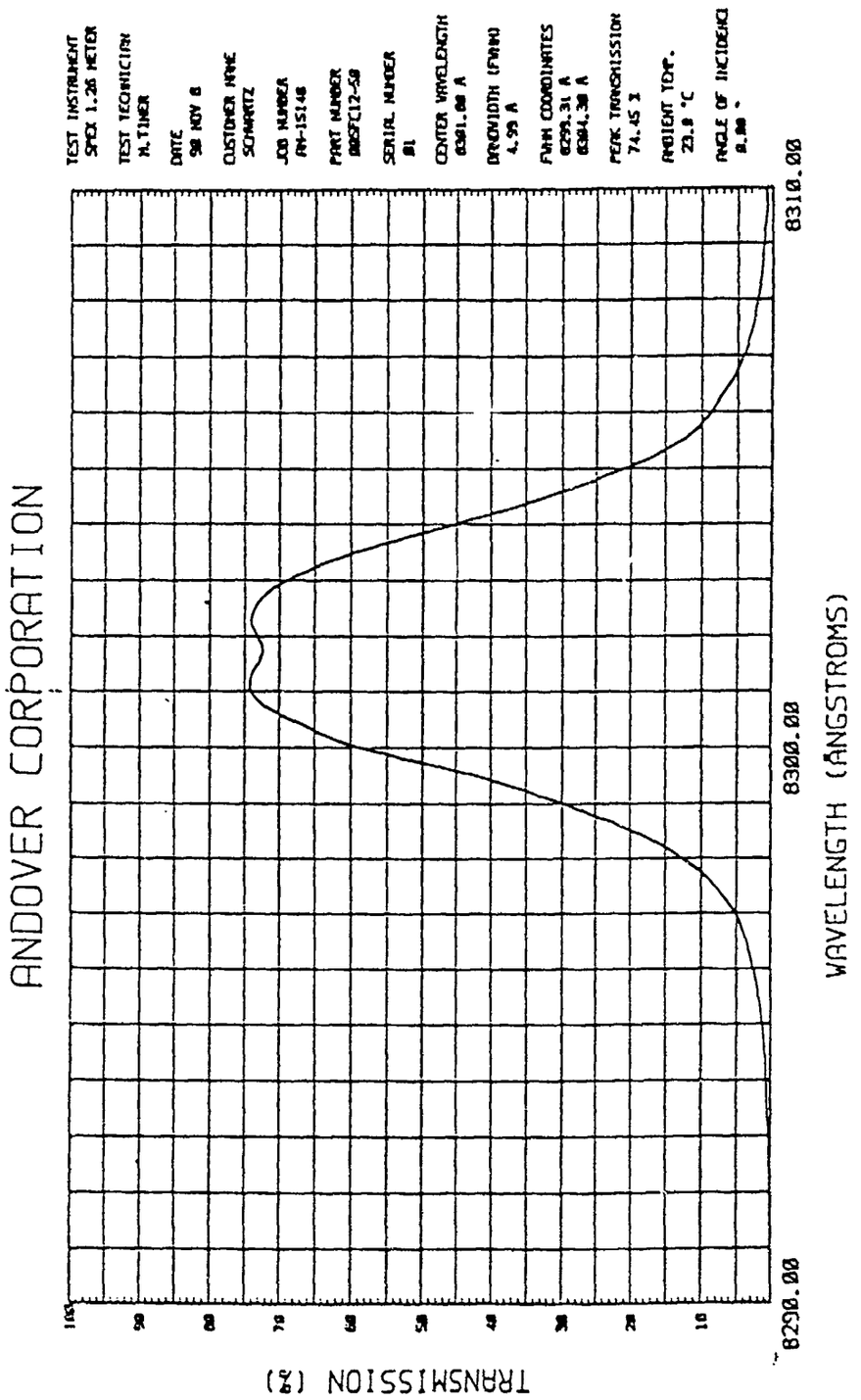

Figure 8. Filter transmission curve at 830 nm

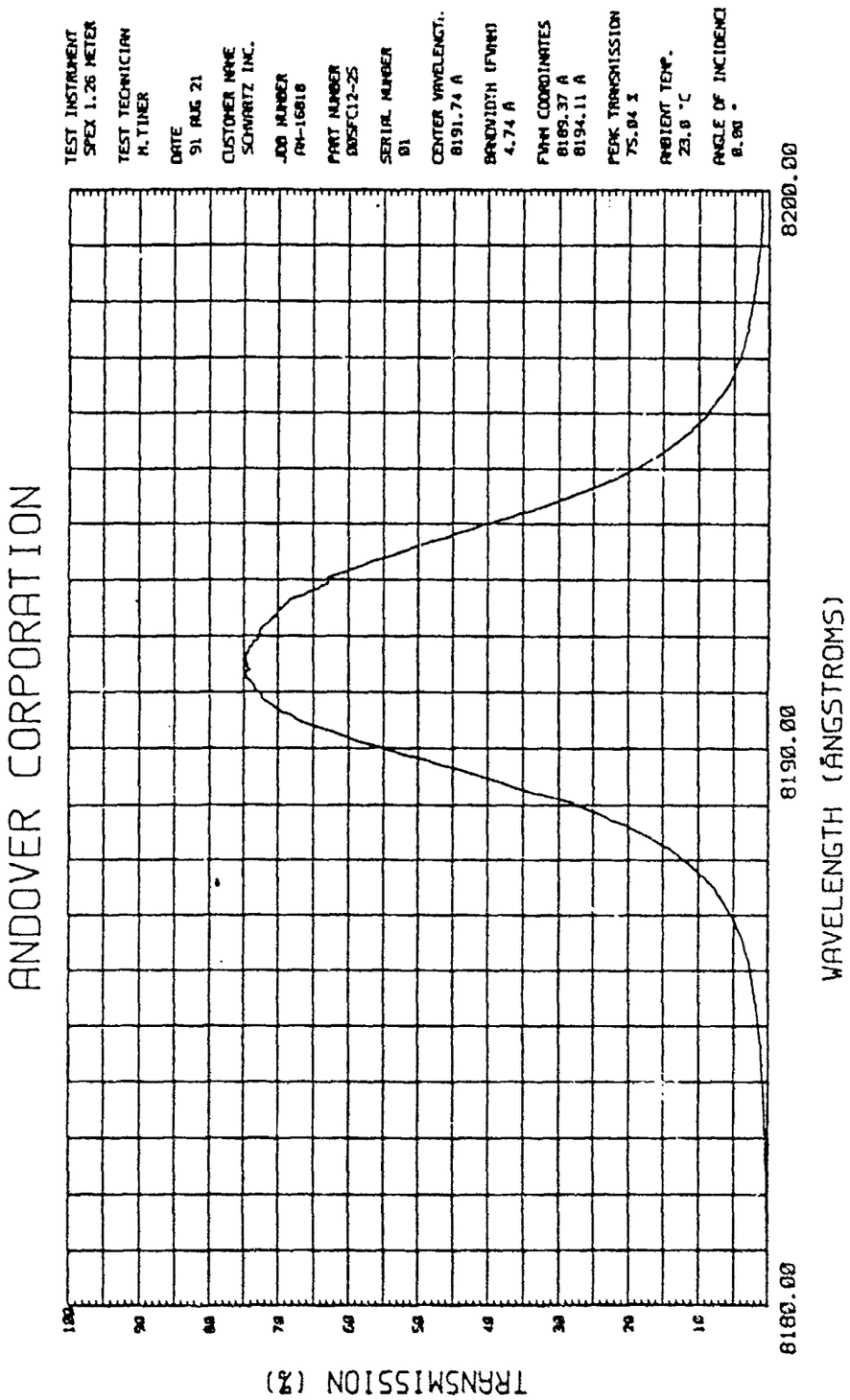

Figure 9. Filter transmission curve at 820 nm

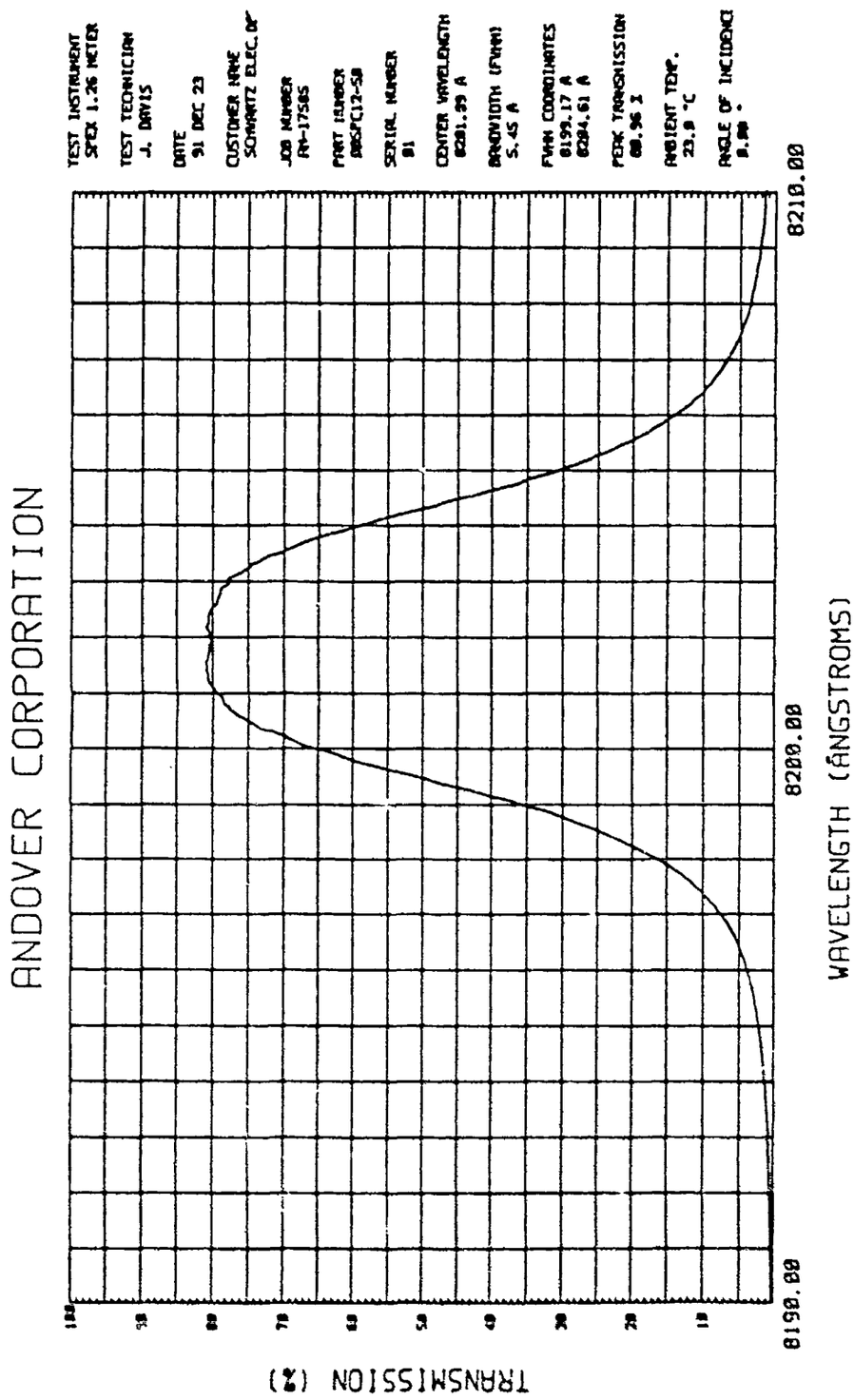

Figure 10. Filter transmission curve at 820 nm

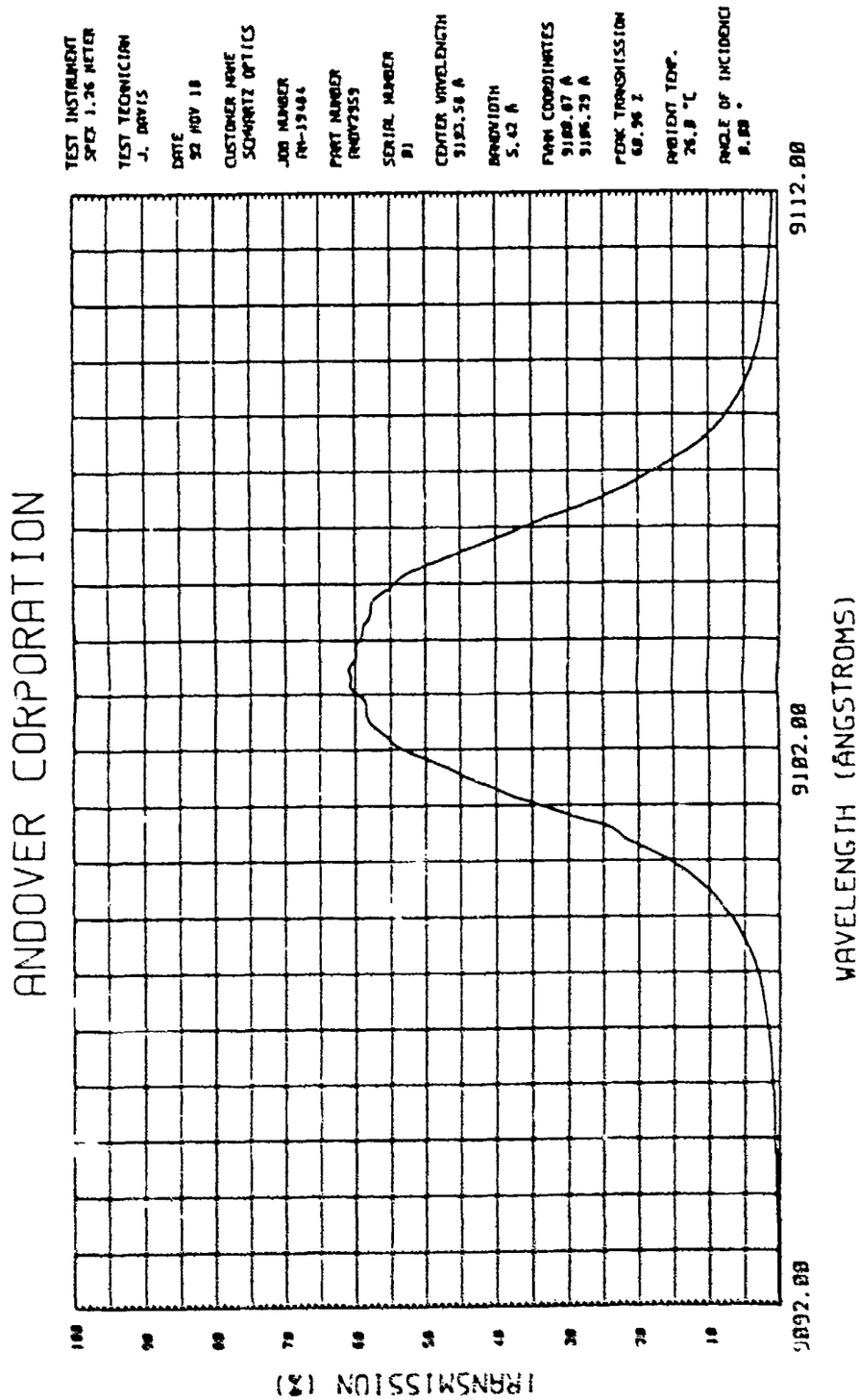

Figure 11 Filter transmission curve at 910 nm

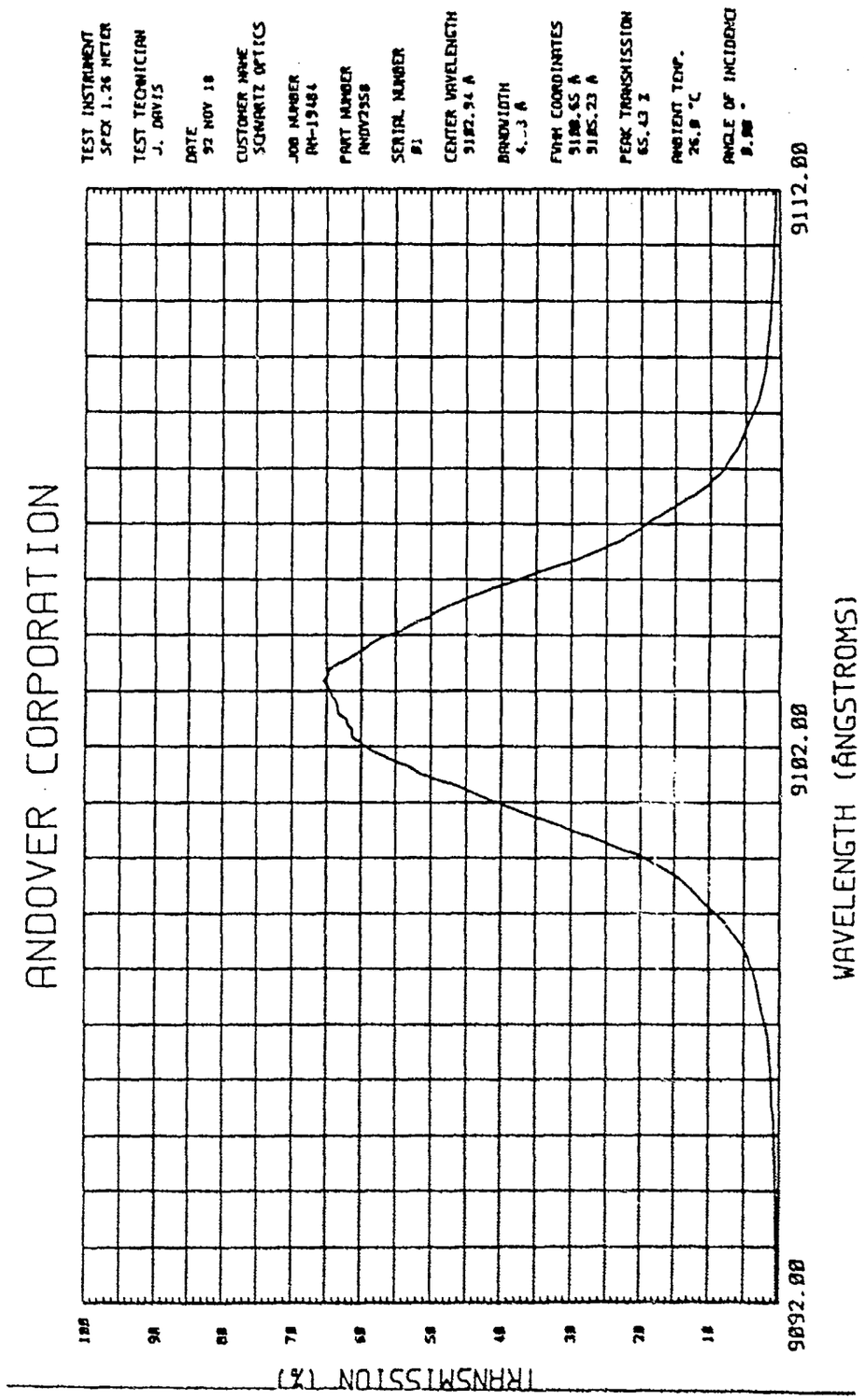

Figure 12. Filter transmission curve at 910 nm

c. External-Cavity Diode Laser

Work on the laser transmitter was conducted on a 1' x 2' breadboard. Rigid mounts were used, and a full cover was added to preserve the alignment and protect the optical components. The laser diode was mounted on a linear translation stage and the output coupler held in a two-axis gimbal mount in order to facilitate fine adjustment of the resonator. The intracavity imaging lens employed in the laser experiment was a Special Optics 54-18-15-835. This multi-element lens provided a superior throughput with minimum induced aberrations. As for the intracavity filter, the closest matching filter to the diode laser was chosen. Figure 13 shows the schematic of the external-cavity diode laser experimental setup.

The external-cavity diode laser was assembled and tested using one of the first AR-coated diode lasers. The first attempt at lasing with the external-cavity diode laser was unsuccessful. It was determined that the problem was most likely optical misalignment. Due to the high aspect ratio of the diode laser (0.08 mils x 10 mils) the positions of the lens and output mirror were very critical.

Measurements of the line-narrowed characteristics of the diode lasers were attempted using the filters within the external cavity. Great difficulty was encountered with the diodes because they exhibited dark stripes along the output, perpendicular to the p-n junction. It was impossible to obtain feedback across the full gain region, and therefore, good efficiency from the external cavity was not achieved. The diode with which the following data were obtained, for instance, had a single dark spot in the center of the output when new. The spatial profile degraded over time so that there were five dark strips. Translation of the collimating lens parallel to the p-n junction, combined with output coupler alignment, produced strong lasing on different spots but never on all of them simultaneously It is possible that some of the degradation in this device occurred during output coupling optimization experiments The initial observation of feedback control was made using a 95% R mirror, and maybe the high level of feedback caused some early damage The original dark spot increased in size; the strips occurred later

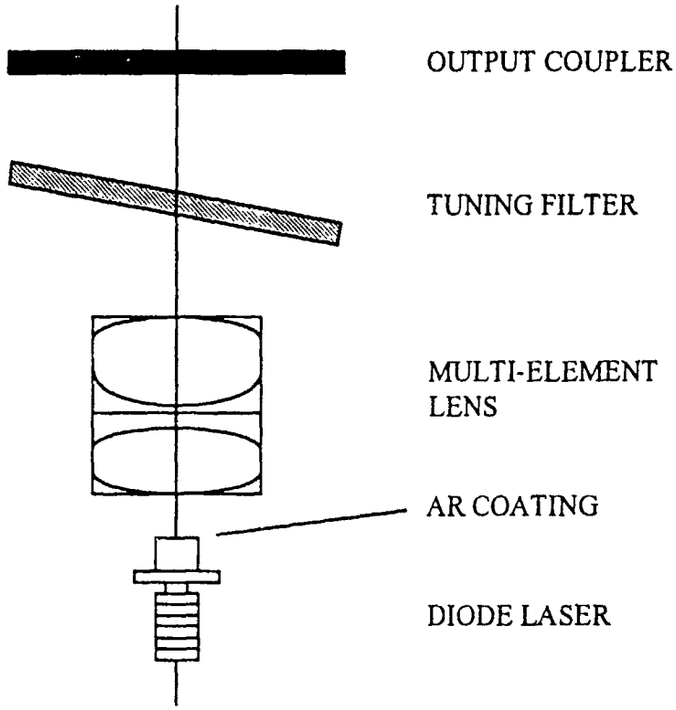

Figure 13. Original line narrowing optical setup

Subsequently, feedback control was observed with only 3-5% R. The data were collected using a 40% R mirror.

Diode 1629I #2 (with center wavelength at 820 nm) was used for the following I/O measurements. Pulse energy was measured using the SEO LTE1003 calibrated power meter. Figure 14 shows the output power vs. drive current for the device with only the collimating lens inserted. Figure 15 shows output power vs. drive current with the 40% R output coupler added (misaligned and aligned). Figure 16 shows output power vs. drive current with the intra-cavity narrow-bandwidth filter added (output coupler misaligned and aligned). Figure 10 shows the filter transmission curve was with the diode lasers having a center wave length of 820 nm.

Measurements of the linewidth of the device 1629H #1 (with center wavelength at 820 nm) in different configurations are shown in Figures 17, 18, and 19. The output signal of a 2048-element photodiode array, placed at the exit of a 0.64 m grating spectrometer, was displayed on a 9410 LeCroy oscilloscope. Spectral resolution was approximately 2.4 nm per 100 μs. Figure 17 shows that the spectral bandwidth of the collimated AR-coated device was 4.32 nm. Figure 18 shows that the spectral bandwidth of the AR-coated device in an external cavity was 2.4 nm. Figure 19 shows that the spectral bandwidth of the AR-coated device in an external cavity with an intra-cavity bandpass filter was 4.8 angstroms.

The spectral data along with the output power of the diode lasers point up the enhancement in spectral brightness realized by using an external cavity which includes an intra-cavity line-narrowing filter. Comparative values are given in Table 1. The peak optical power measured from the collimated diode laser was 12.5 W. The peak optical power measured with the diode laser in an external cavity was 8.25 W. The peak optical power measured with diode laser in an external cavity with an intra-cavity bandbass filter was 5 W. The spectral power density of the collimated diode laser was 0.29 W/Å. The spectral power density of the diode laser in an external cavity was 0.34 W/Å. The spectal power density of the diode laser in an external cavity with an intra-cavity filter was 1.04 W/Å.

Due to the rapid degradation of the LDL AR-coated devices, several diode lasers were purchased from Ensign Bickford Aerospace Co. (EBAC) and AR-coated at M.I.T.-Lincoln Laboratory. The EBAC diode lasers had center wavelengths at 820 nm (see Figure 10 for the transmission curve of the intra-cavity filter used to test the EBAC diode lasers). The oscilloscope traces in Figures 20-23 show temporal (10 ns/DIV) and spectral (2.33×10^{-2} nm/μs) characteristics that are typical of those obtained with the AR-coated diode lasers. The measured FWHM pulse width of 27 ns was broadened slightly due to the detector bandwidth (Figure 20). Without feedback (Figure 21), the FWHM spectral width was 2.9 nm. With feedback (Figure 22), the spectrum was narrowed to 2 nm. With the intracavity filter and feedback (Figure 23), this was reduced to 0.33 nm. The corresponding reductions in peak power were 1% and 5% with and without feedback (using 95% T output coupler and no intracavity filter) and 37% with both

filter) and 37% with both the filter and feedback. All of the data included were obtained with the power supply set at 20V, the temperature of the diode laser maintained at 27°C, and a 1 kHz pulse repetition rate. It is interesting to note that lower transmission output couplers (as low as 50% T) provided no observable improvement in spectral narrowing. The test data in Table 2 show the dependence of the peak power upon supply voltage with the output coupler misaligned and optimally aligned for feedback.

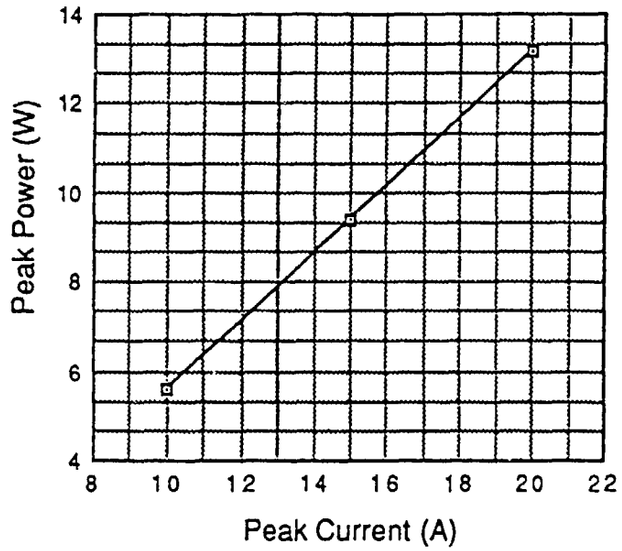

Figure 14. Output power curve for collimated laser diode

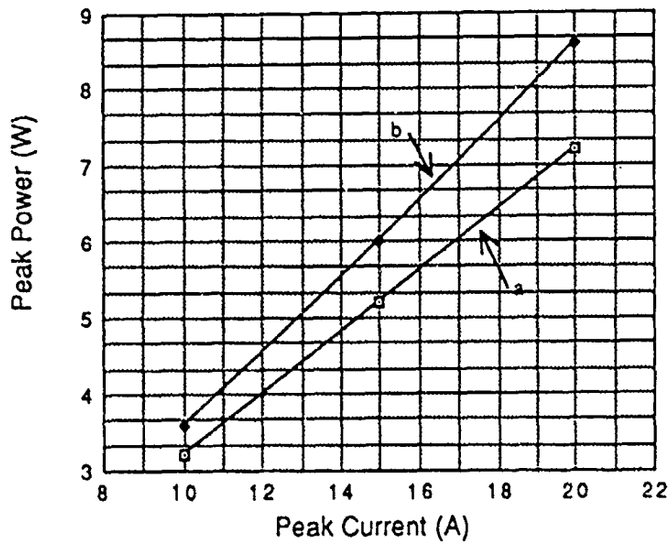

Figure 15. Output power curve for output coupler misaligned (curve a), and output coupler aligned (curve b) with external cavity

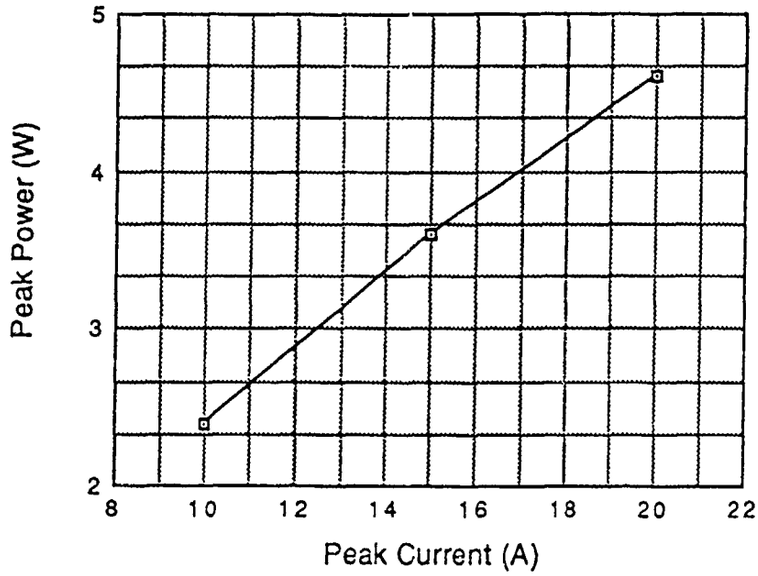

Figure 16. Output power curve for the external cavity with an intra-cavity filter

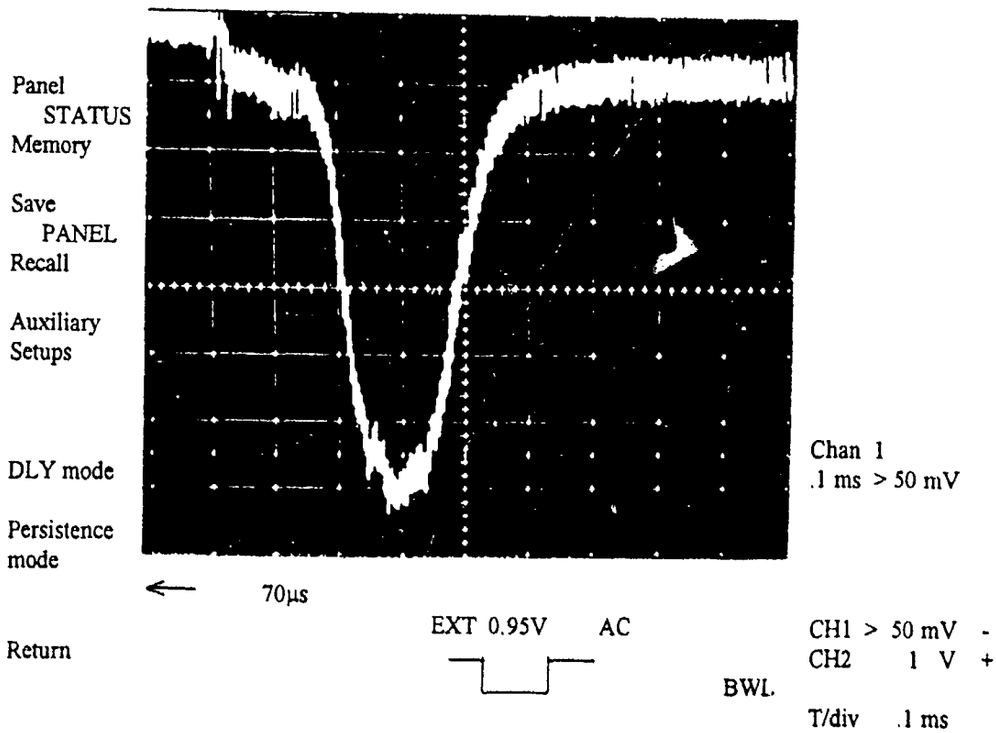

Figure 17. Spectral characteristics of the collimated AR-coated device

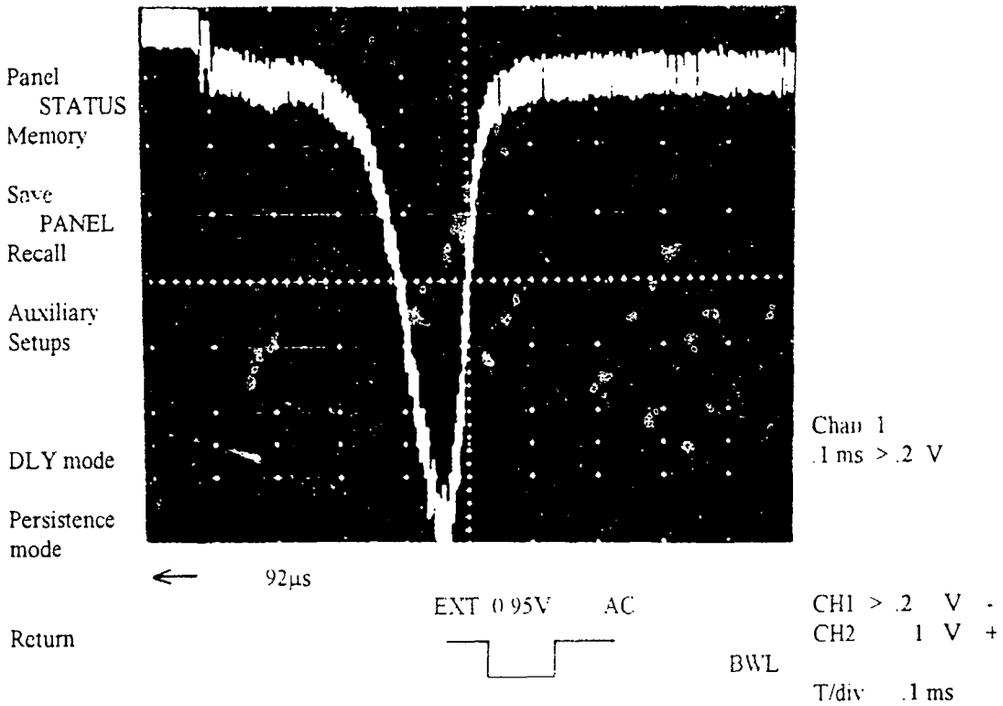

Figure 18. Spectral characteristics of the AR-coated device in an external cavity

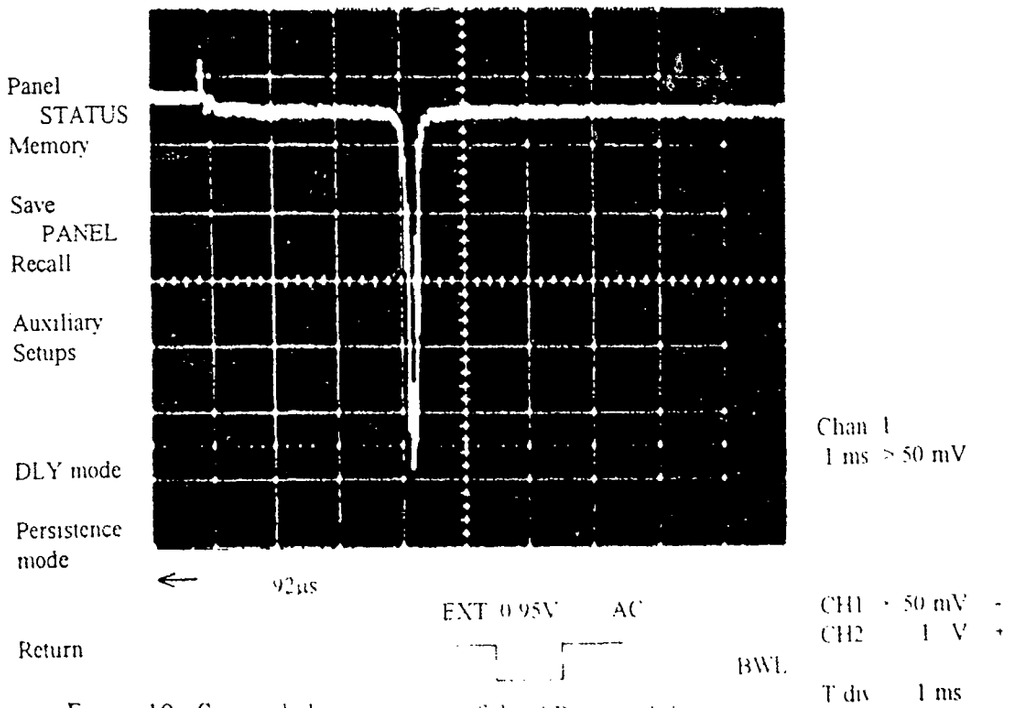

Figure 19 Spectral characteristics of the AR-coated device in an external cavity with an intra-cavity bandpass filter

Table 1. Diode laser power and bandwidth data

DEVICE	OPTICAL PEAK POWER (W)	SPECTRAL BANDWIDTH (Å)	SPECTRAL POWER DENSITY (W/Å)
Collimated Laser Diode	12.5	43.2	0.29
Laser Diode X-Cavity	8.25	24	0.34
X-Cavity w/ filter	5	4.8	1.04

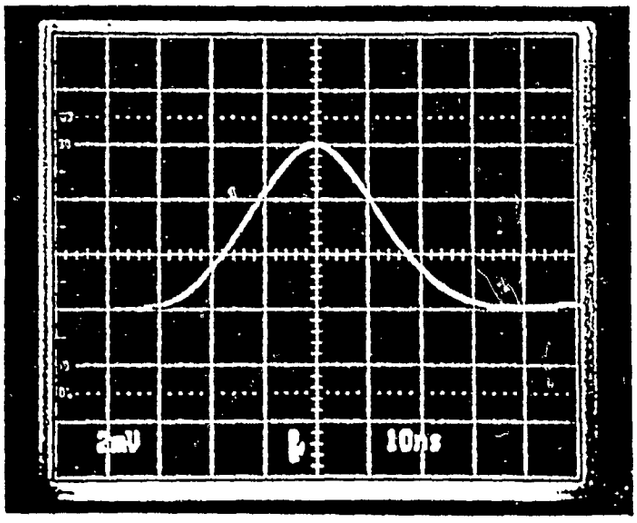

Figure 20. Measured pulse width with 2" filter

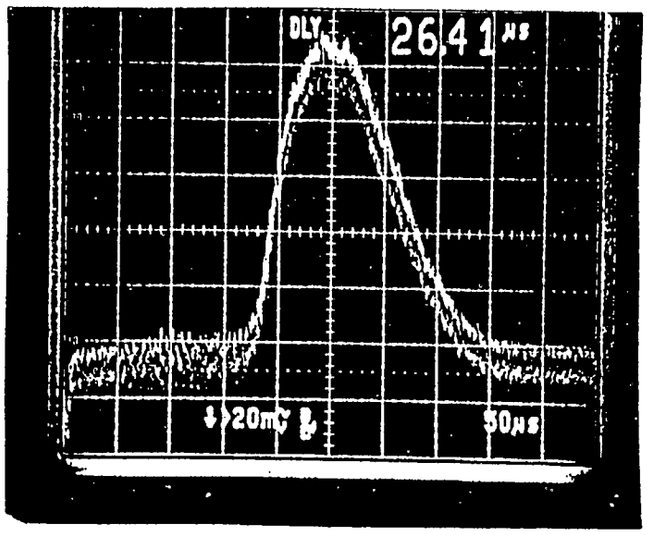

Figure 21. Spectral width without filter

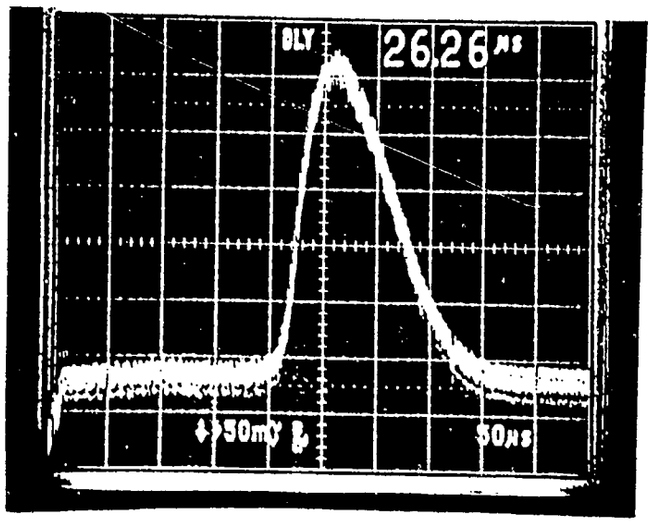

Figure 22. Spectral width with feedback

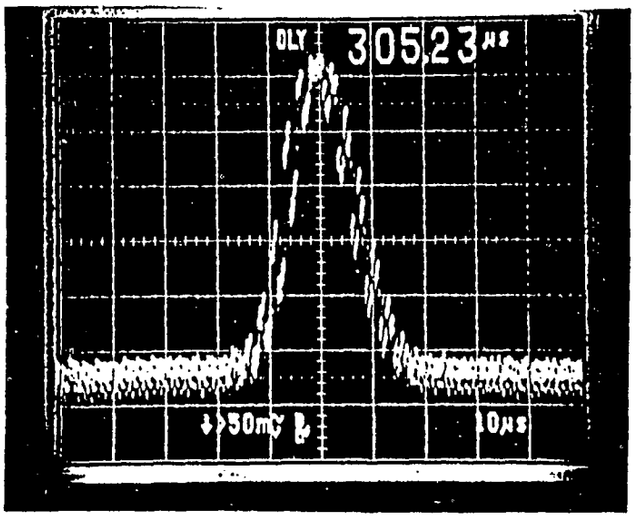

Figure 23. Spectral width with intra-cavity filter & feedback

Above a power-supply setting of 30V (corresponding to ≃ 30 A peak current), the EBAC diode laser exhibited immediate failure, typically characterized by a dark line in the center of the normally uniform far-field emission pattern (perpendicular to the junction) with a severe reduction in output power. This was observed both with the AR-coated lasers and with the single device obtained with the standard EBAC coating.

Measurements of threshold currents provided by EBAC indicate that the AR-coating reflectivities were considerably in excess of 1%. In this case, the AR-coated diode lasers would apparently offer no operational advantage over standard devices. The line narrowing technique was tested on off-the-shelf diode lasers from LDL (CVD-62) under the following conditions:

Conditions of the test: Laser Temp. = 27°C
Laser High Voltage = 32.5 V

CVD-62 specifications: $\lambda_c = 905$ nm $\pm$ 10 nm (see Figure 12)

$\Delta\lambda_{FHWM} = 5$ nm Typ.

$\phi_{pk} = 9$ W Typ.

Spectral filter specifications: $\lambda_c = 910.294$ nm

$\Delta\lambda_{FWHM} = 0.458$ nm

$T_{pk} = 65.43\%$

The raw, collimated, peak output power measured was 8.13 W. The peak output power measured after the collimating lens and spectral filter was 0.63 W. The peak output power measured after the collimating lens and with 20% R output coupler (without filter) was 6.49 W.

Table 2. Peak power vs. supply voltage with the output coupler misaligned and optimally aligned for feedback

SUPPLY VOLTAGE (V)	PEAK POWER w/o FEEDBACK (W)	PEAK POWER w/ FEEDBACK (W)
5	1.23	0.85
10	3.23	2.31
15	5.31	3.54
20	7.01	4.62

Various output couplers were tested to determine the best mirror to use for maximum output power and spectral bandwidth narrowing. Table 3 shows the results of the various output couplers. The poor efficiency was the result of low filter transmission. Figure 24 shows the spectral bandwidth of the line-narrowed CVD-62 using different output couplers.

In pursuit of higher peak output power, the laser transmitter optical setup was modified as shown in Figure 25. A 50/50 beam splitter was added so that only half of the diode laser output was reflected to the external cavity while the other half (A) was transmitted. In addition, a folding mirror was used to redirect the beam (B) from the external cavity which was transmitted by the beam splitter. The highest peak output power that was obtained from the original configuration, was 1.85 W; with the modified configuration, we obtained 5.61 W (4.32 W from the main output plus 1.29 W from the folding mirror) was obtained. Table 4 lists the output power and spectral bandwidth at various locations denoted in the optical setup of Figure 25.

Table 3. Test results with various output couplers

OUTPUT COUPLER	PEAK OUTPUT POWER (W)	$\Delta\lambda_{FWHM}$ (Å)	EFFICIENCY (%)
10 % R	1.72	2.51	21.2
20 % R	1.85	2.8	22.8
30 % R	1.64	2.88	20.2
50 % R	1.25	2.56	15.4

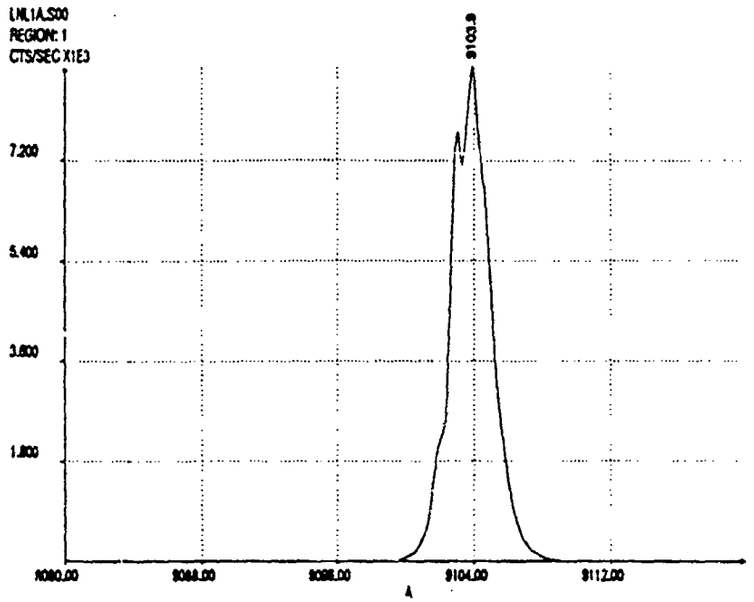

A. $\Delta\lambda_{FWHM} = 2.51$Å with 10% O.C.

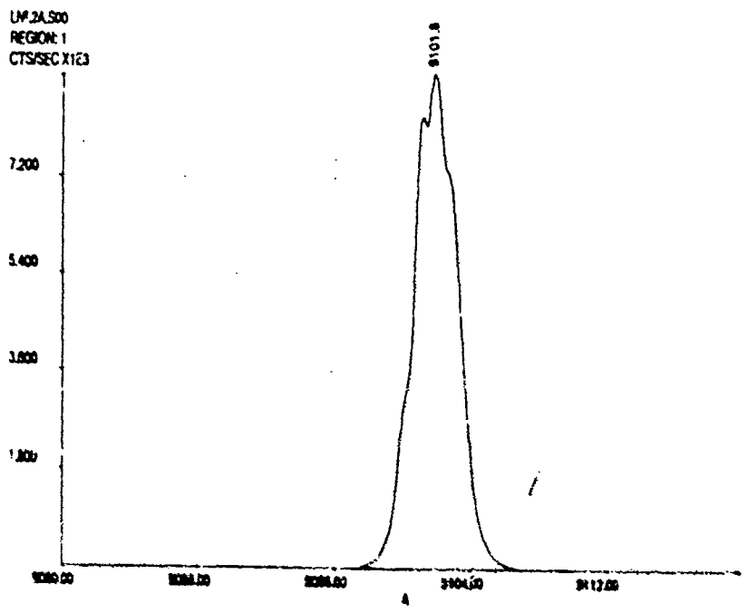

B. $\Delta\lambda_{FWHM} = 2.80$Å with 20% O.C.

Figure 24. Spectral bandwidth of the CVD-62 versus output coupler transmission

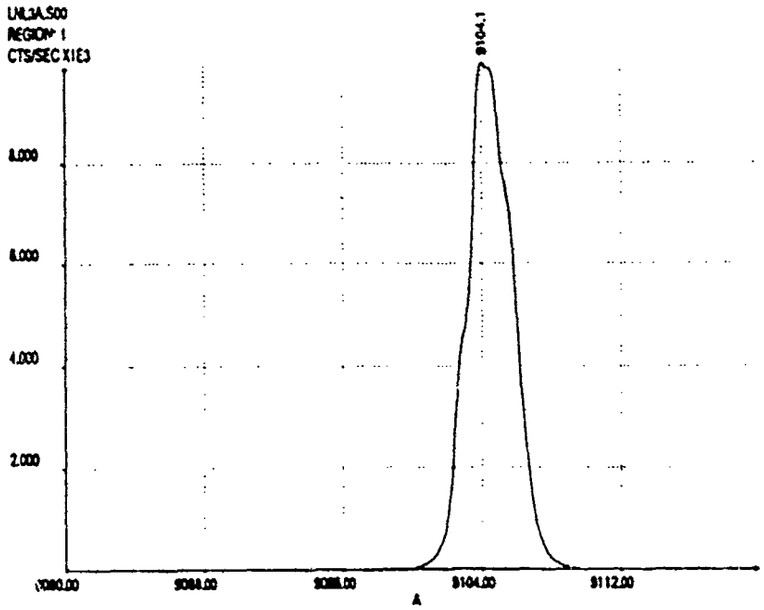

C. $\Delta\lambda_{FWHM} = 2.88$Å with 30% O.C.

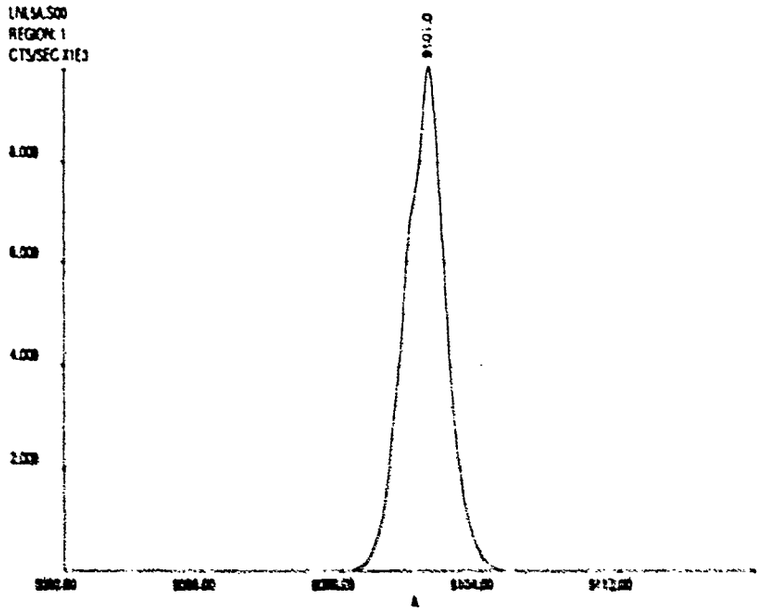

D. $\Delta\lambda_{FWHM} = 2.56$Å with 50% O.C.

Figure 24 Spectral bandwidth of the CVD-62 versus output coupler transmission

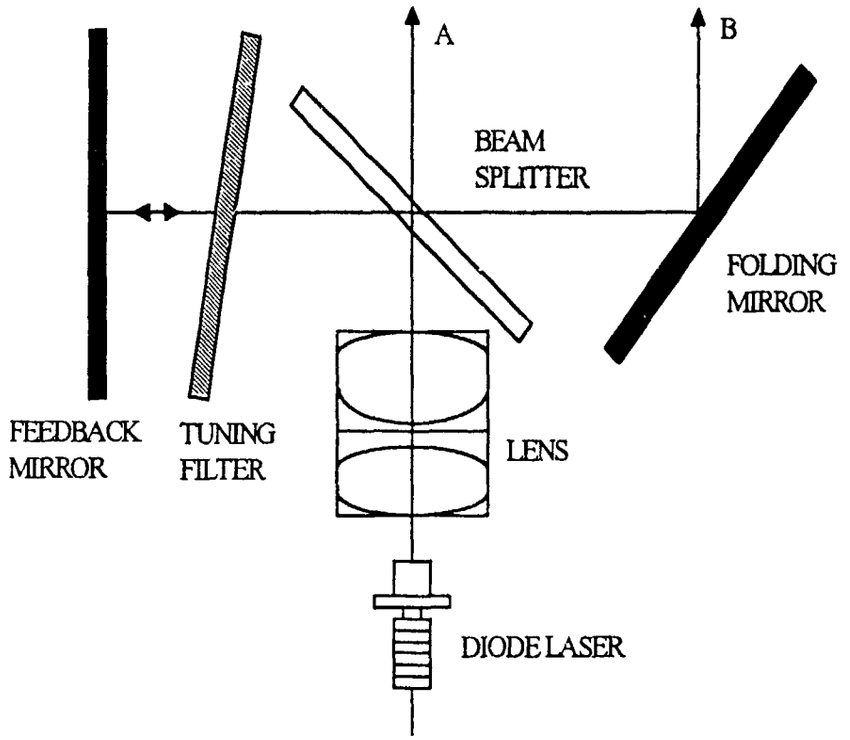

Figure 25. Modified line-narrowing optical setup

Table 4. Output power and spectral bandwidth at various locations

MEASUREMENT LOCATION (Figure 25)	OUTPUT PEAK POWER (W)	SPECTRAL BANDWIDTH (Å)	OPTICAL POWER EFFICIENCY (%)
A	4.32	3.44	53.13
B	1.29	2.67	15.87
A & B	5.61	- -	69.01

2. LINE-NARROWED DIODE-LASER RANGE FINDER

a. System Design

A block diagram of the single-channel line-narrowed range finder is presented in Figure 26. This pulsed time-of-flight type range finder was designed to measure range to non-cooperative (10% Lambertian) targets at a maximum range of approximately 200 m with a range resolution of 10 cm. The range finder is comprised of four subsystems -- laser transmitter, optical receiver, range counter, and computer -- which are described in the following paragraphs.

The transmitter consists of a diode laser and pulser. The GaAlAs metal organic chemical vapor deposition (MOCVD) diode laser emits 6 ns (FWHM) light pulses at a wavelength of 910 nm and a repetition rate of 1 kHz. The diode laser is driven with 20 A current pulses, which are produced by a metal-oxide-semiconductor field-effect transistor (MOSFET).

The optical receiver block diagram is depicted in Figure 27. The optical detection circuitry is dedicated specifically to the function of converting optical irradiance to first, an equivalent electrical analog of the input irradiance, and finally, a logic-level signal. Logic level signals are then processed within the range counter logic to yield digital target-range data.

An avalanche photodiode detector (APD) is used to detect the laser return pulse reflected by a target. The APD is a reverse-biased junction photodetector in which photogenerated charge carriers are accelerated by the bias and generate further carriers by impact ionization. The APD used in the single-channel sensor is an EG&G C30902E. The active diameter of this APD is 0.5 mm. The response time of the device is less than one nanosecond. The rms noise current of this device, when operating with a gain of 100, is only $2.3 \times 10^{-13}\ A/\sqrt{Hz}$.

The APD operates as a current source in conjunction with a transimpedance amplifier. The transimpedance amplifier operation produces a near "zero" (typically 200 ohms) node at the input terminal, thus, no significant voltage excursion occurs across the detector and system

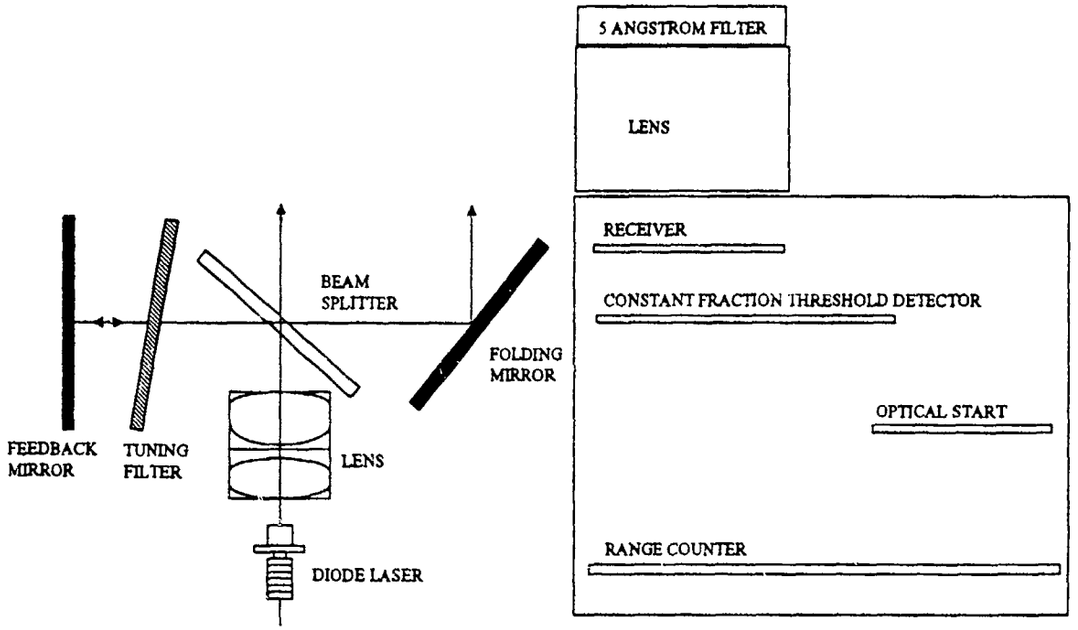

Figure 26. Line-narrowed range finder

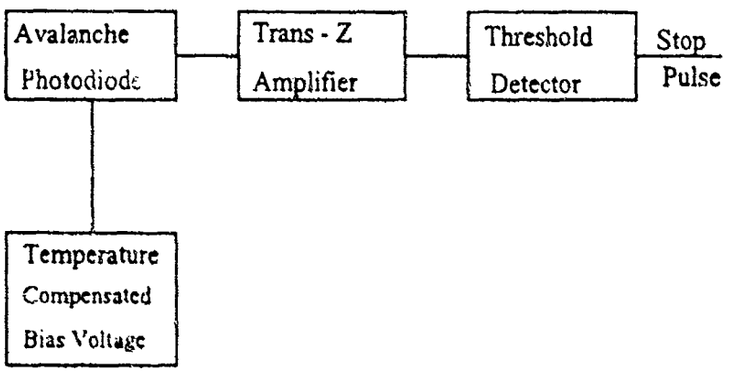

Figure 27. Optical receiver block diagram

bandwidth is retained. The transimpedance amplifier is the NE5211. This component offers transimpedance of 28 kΩ when operated in the differential mode. The input noise current contribution of the transimpedance amplifier is approximately 1.8 pA/$\sqrt{Hz}$.

It is significant to note that the bias voltage at avalanche varies widely with junction temperature variation. The C30902E bias voltage may range from as little as 190 V, for cold conditions, to as great as 250 V for a junction temperature of +70°C. A temperature-compensated high-voltage supply is used to maintain the correct reverse bias on the APD.

The start timing pulse is produced using optical detection of the transmitter laser pulse, which decreases the time error caused by delay changes in the diode laser. An optical fiber between the diode laser and the p-i-n diode is used for the start pulse detection.

A block diagram of the range-measurement circuit is presented in Figure 28. At the time of transmitting the laser pulse, an electronic switch is closed, causing an energy-storage capacitor to be charged by a constant-current source. When the return pulse is received, the electronic switch is opened. The voltage across the capacitor is proportional to the charging-time interval, i.e., the propagation time to and from the target. At the time of the received pulse, the capacitor voltage is transferred to a sample-and-hold circuit. Then the capacitor is discharged to await another transmit-pulse signal. If a return pulse is not received within the allotted time, a sample is not taken and the last pulse is held. This technique is basically an analog technique and as such is limited to an accuracy of about 1% of the full scale. This accuracy limitation is due to variation of the constant-current source, sample-and-hold gain variation, capacitor variation and averaging-amplifier gain variation over the temperature range. These variations are not random, but produce a positive or negative bias in the range reading. When limited to shorter range (<300 m) systems, this technique has a resolution of 6 to 8 cm.

The final component of the range finder is a IBM portable computer (PC) with I/O card and range display software. The I/O card reads the data from the A/D converter of the Range Counter circuit. The software collects the range data and displays the following information: total counts, total valid counts, minimum range, maximum range, average range, standard deviation, and percent of probable detection.

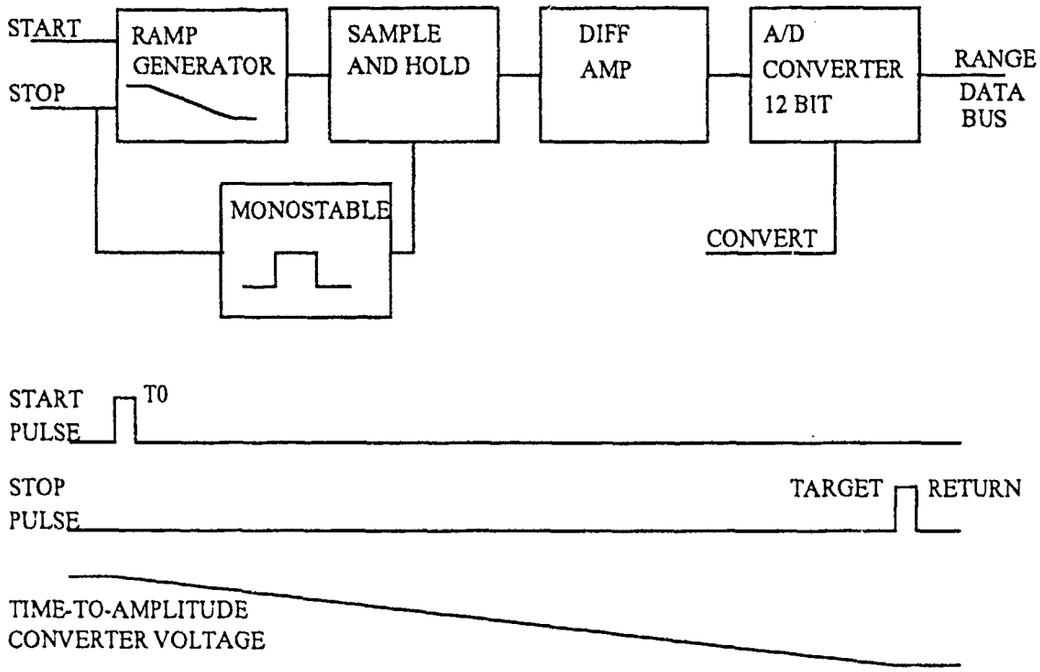

Figure 28. Analog range counter block diagram

b. System Tests

The first range test was conducted with the modified line-narrowed system shown schematically in Figure 26. Measured range data are compiled in Table 5. Figure 29 shows the computer-simulated maximum range for the line-narrowed system.

Table 5. Test results from line-narrowed system

Optical Output Peak Power: 5.61 W

Conditions: Scattered Clouds, Mostly Sunny, Temp. 75 - 80 deg. F.

Time: 2:00 PM - 3:30 PM

Target Type: White Plywood (2' x 8')

Range Data

Samples/Channel: 100 Scale: 0.29304 (ft/bit)

COUNT		RANGE (ft)					ACTUAL RANGE (ft)
Total	Valid	Average	Min	Max	Std Dev	%%PD	
100	100	134.48	133.92	135.38	0.28	100	124
100	100	238.09	225.35	269.89	8.62	100	224
100	100	317.98	317.36	318.53	0.22	100	324
100	100	377.89	364.26	394.14	3.99	100	374
100	100	424.22	419.63	441.03	3.62	100	424
100	100	470.24	455.68	484.98	3.33	100	474
100	99	480.65	473.26	675.16	20.18	99	484

```
System Name: 1025                                                    03-18-1993
Receiver Parameters
 5      cm     Receiver aperture          | 2.5e-12        Amp equiv noise crrnt den
 .92           Xmission thru rcvr optics  | 1.33e-13       Detector dark crrnt, bulk
 .61           Xmission through filter    | 1e-8           Detector dark crrnt, srfc
 5      A      Optical filter bandwidth   | .53    A/W     Detector responsivity,M=1
 100    MHz    Receiver bandwidth         | 10     mr      Field of view
 132           APD gain

System Parameters
 .1            Reflectance of target      | .01            Probabilty of false alarm
 .3            Reflectance of background  | .99            Probability of detection
 .12    /km    Atmospheric ext. coeff.    | 800            Solar Spectral Irradiance
 50     ft     Minimum Range Gate         | 0              Cant Angle in degrees

Laser Parameters
 .7            Collection efficiency      | 13     W       Laser diode output power
 .6            Xmssion thru Xmtter optcs

Max. Range =    465 ft,  142 M        SNR  = 17.07 dB       Accuracy = +/- 0.23 ft
Signal Power = 9.21E-09 Watts         TNR  =  4.23                   = +/- 0.07 M
Solar  Power = 3.25E-09 Watts   Vsig = 4.83 mV   Vnoise = 0.67 mV    Mopt = 132
 Edit (R)cvr param, Edit (S)ys param, Edit (L)aser param, (C)alculate, (Q)uit:
```

Figure 29. Computer-simulated data for the line-narrowed range finder

A second range test was conducted with the conventional range finder system shown in Figure 30. Measured range data are complied in Table 6. Figure 31 shows the computer-simulated maximum range for the conventional system.

Comparing the range test data of the line-narrowed system and conventional range finder system, the line-narrowed system was able to range to 484 ft with 5.61 W peak output power while the conventional system was able to range to 324 ft with 8.13 W peak output power. The line-narrowed system was able to range farther than the conventional system because the spectral energy density of the line-narrowed system (2.08 W/Å) was greater than the conventional system (0.16 W/Å). The variations between the range data and the actual range were due to parallax. The largest range variation was at the shorter ranges where the parallax was the greatest, and the smallest range variation was at the longer ranges where the parallax was the least.

Table 6. Test results from conventional system

Optical Output Peak Power: 8.13 W

Conditions: Mostly Cloudy, Temp. 80 - 85 deg. F.

Time: 2:00 PM - 3:00 PM

Target Type: White Plywood (2' x 8')

Range Data

Samples/Channel: 100 Scale: 0.29304 (ft/bit)

COUNT		RANGE (ft)					ACTUAL RANGE (ft)
Total	Valid	Average	Min	Max	Std Dev	%%PD	
100	100	137.1	136.56	138.02	0.25	100	124
100	100	229.59	229.16	230.62	0.27	100	224
100	100	335.66	332.31	348.13	2.9	100	324

Target Type: Black Plywood (2' x 8')

Range Data

Samples/Channel: 100 Scale: 0.29304 (ft/bit)

COUNT		RANGE (ft)					ACTUAL RANGE (ft)
Total	Valid	Average	Min	Max	Std Dev	%%PD	
100	100	136.99	136.56	137.73	0.27	100	124
100	100	183.29	182.56	184.91	0.46	100	174
100	100	240.34	227.99	258.46	5.95	100	224

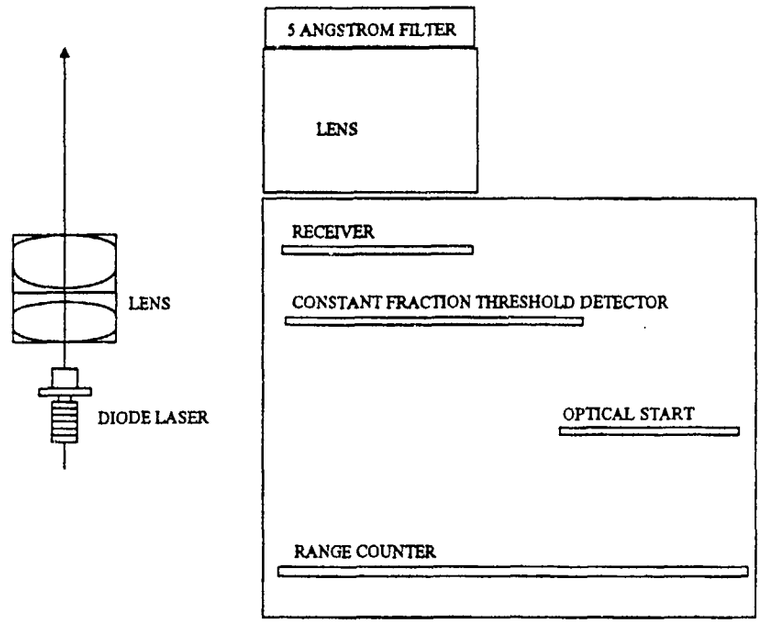

Figure 30. Conventional range finder

```
System Name: 1025                                                    03-18-1993
Receiver Parameters
 5      cm     Receiver aperture          | 2.5e-12        Amp equiv noise crrnt den
 .92           Xmission thru rcvr optics  | 1.33e-13       Detector dark crrnt, bulk
 .61           Xmission through filter    | 1e-8           Detector dark crrnt, srfc
 400    A      Optical filter bandwidth   | .53    A/W     Detector responsivity,M=1
 100    MHz    Receiver bandwidth         | 10     mr      Field of view
 20            APD gain                   |
System Parameters
 .1            Reflectance of target.     | .01            Probabilty of false alarm
 .3            Reflectance of background  | .99            Probability of detection
 .12    /km    Atmospheric ext. coeff.    | 800            Solar Spectral Irradiance
 50     ft     Minimum Range Gate         | 0              Cant Angle in degrees
Laser Parameters
 .7            Collection efficiency      | 13       W     Laser diode output power
 .92           Xmssion thru Xmtter optcs  |
Max. Range =     230 ft,    70 M        SNR  = 16.82 dB       Accuracy = +/- 0.24 ft
Signal Power = 5.88E-08 Watts           TNR  =  4.03                   = +/- 0.07 M
Solar  Power = 2.62E-07 Watts   Vsig = 4.67 mV   Vnoise = 0.65 mV    Mopt =  20
 Edit (R)cvr param, Edit (S)ys param, Edit (L)aser param, (C)a)culate, (Q)uit:
```

Figure 31. Computer-simulated data for the line-narrowed range finder

3. MULTI-ELEMENT LASER SOURCE DEVELOPMENT

Even with the enhanced performance that line narrowing brings, the LIRS requires a diode-laser source of about 30 W peak power in order to measure ranges on the order of 1500 to 2000 ft. Since it takes several laser diode elements to generate this much power, a scheme for spatially multiplexing the beams in the external laser cavity is needed. It is apparent from Figure 32 that simply stacking the elements linearly in the focal plane of a single collimating lens provides feedback only for the on-axis element.

The technique of using GRIN lenses to collimate each element of a diode array, thereby achieving parallel beams which can be reflected back on themselves to provide optical feedback, is shown schematically in Figure 33. The 0.23 pitch GRIN lens is designed so that its focal point is outside the entrance face of the lens and a collimated beam is projected from the exit face. The length of the lens is given by

$$Z = \frac{2\pi\rho}{\sqrt{A}} \tag{4}$$

where ρ is the pitch and A is the refractive index gradient constant. The distance from the source to the lens is given by

$$l_1 = \left[N_0 \sqrt{A} \tan\left(\sqrt{A}\, Z\right) \right]^{-1} \tag{5}$$

where N_0 is the on-axis value of the refractive index. The effective focal length of the GRIN lens is given by

$$EFL = \left[N_0 \sqrt{A} \sin\left(\sqrt{A}\, Z\right) \right]^{-1} \tag{6}$$

The only standard 0.23 pitch lenses available have a diameter of 1.8 mm. At a wavelength of 0.83 μm, N_0 = 1.5986 and the square root of A = 0.601. Equations (4), (5), and (6) can now be solved, yielding Z = 4.35 mm, l_1 = 0.24 mm, and EFL = 1.9 mm.

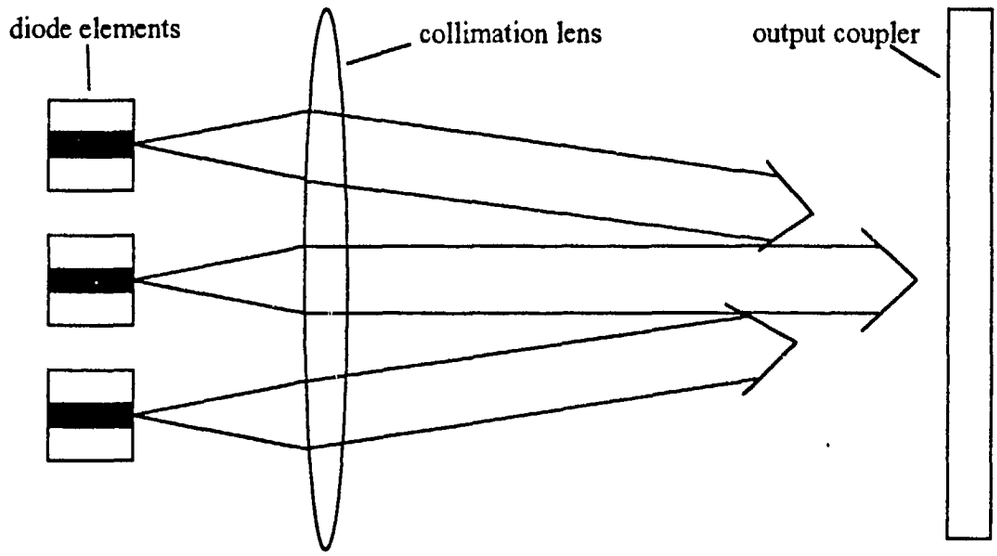

Figure 32. Schematic illustration of resonator misalignment with one collimation lens and multiple diode elements

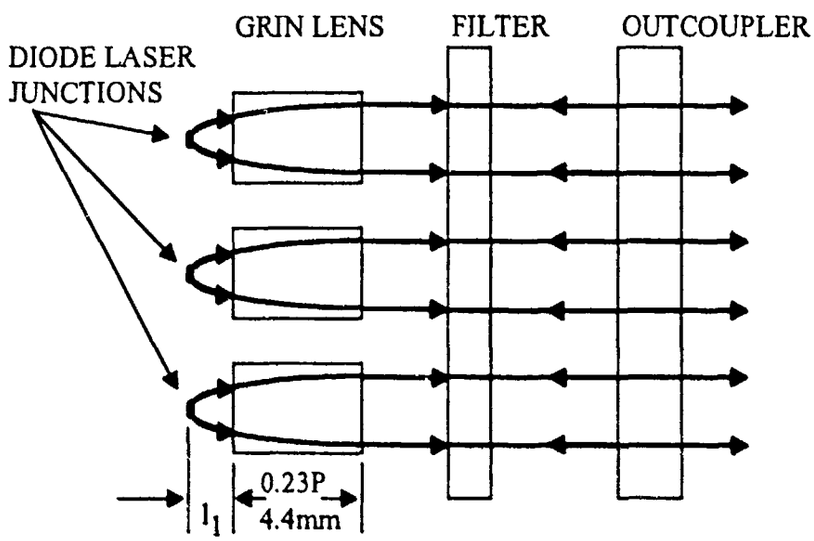

Figure 33. Multi-element line-narrowed diode-laser resonator geometry employing GRIN lens collimators

If the 1.9 mm focal length lens is used to collimate the CVD-62 InGaAs diode laser manufactured by LDL, the collimated beam will have divergence parallel and perpendicular to the junction given by

$$\theta_{||} = \frac{0.152}{1.9} = 0.08 = 4.6^\circ$$

$$\theta_{\perp} = \frac{.001}{1.9} = 0.53\ mrad$$

The 4.6° value of $\theta_{||}$ is too large for use in the LIRS. The divergence could be reduced to a reasonable value by employing a 10x anamorphic beam expander outside the resonator cavity. Another problem with the GRIN lens is its poor off-axis imaging quality which can result in considerable loss when the feedback radiation is reimaged upon the diode element.

The 30 W LIRS requirement can be met using three CVD-62 lasers. Using a Special Optics 54-18-15 lens to collimate each CVD-62 results in efficient ($\simeq$ 80 %) energy collection and an acceptable divergence parallel to the junction: $\theta_{||} = 0.152/15 = 10$ *mrad*. If the diode lasers are mounted in the same plane for ease of excitation and heat sinking, then the collimation lenses must be mounted on X-Y-Z positioners as shown in Figure 34. The three parallel beams in this configuration fit within a 50 mm aperture.

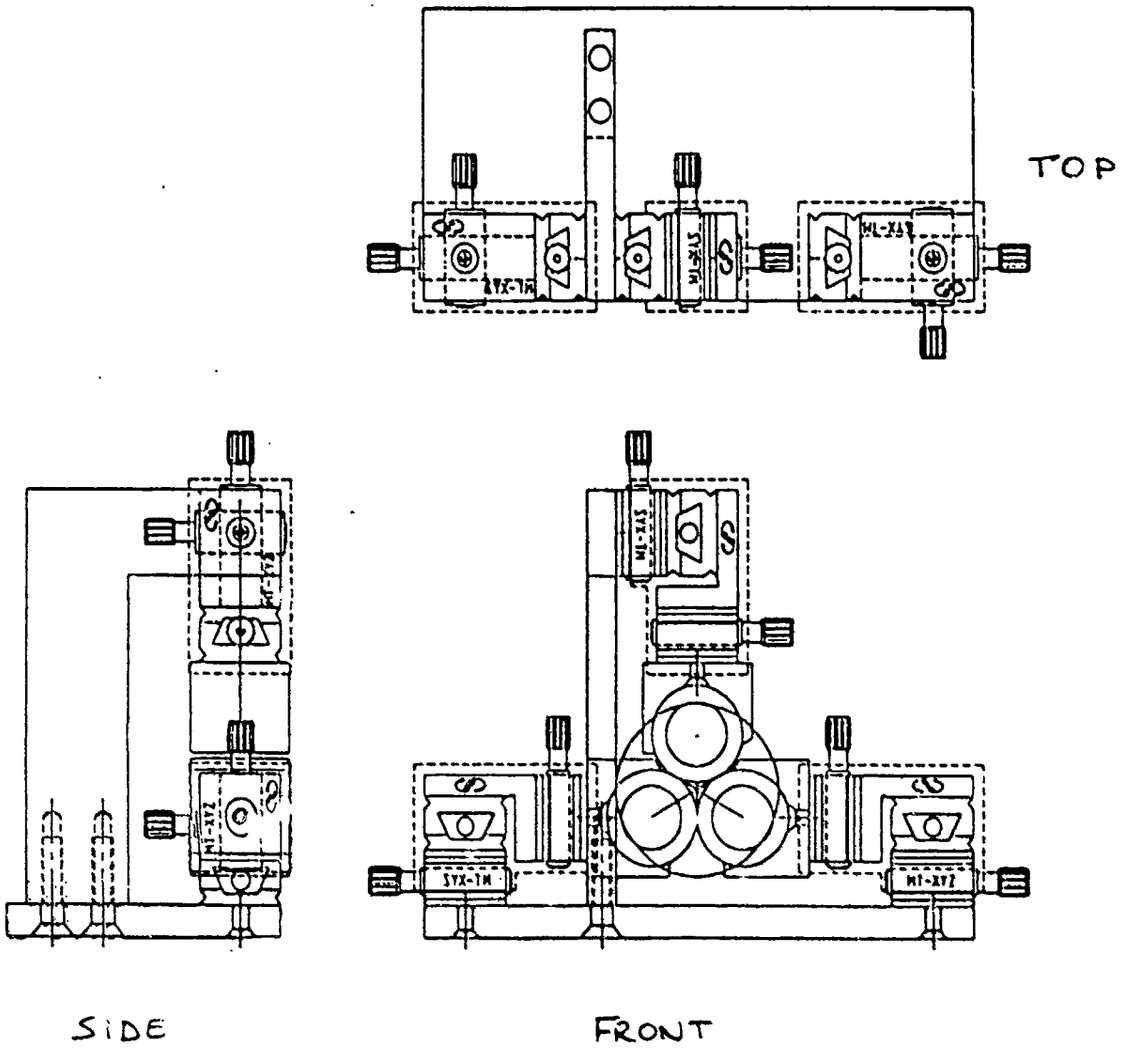

Figure 34. Mounting configuration for three 18-mm aperture collimating lenses

4. DIODE-LASER COLLIMATION VIA CYLINDRICAL MICROLENS

Efficient collection of radiation from and collimation of the fast axis of a diode laser requires the use of a diffraction-limited cylindrical lens having a numerical aperture of about 0.5. Until recently, fast, well-corrected cylindrical lenses were generally unavailable. However, in 1991 Blue Sky Research introduced f/0.9 diffraction-limited microlenses fabricated by drawing optical fibers from shaped glass preforms. These microscopic lenses are potentially more robust and less expensive than macroscopic optics.

In order to evaluate the efficacy of microlens collimation of a diode laser, the setup shown in Figure 35 was used to position the hyperbolic first surface of the cylindrical lens shown in Figure 36 110 μm in front of the emitting surfaces of a twelve-element diode-laser array. A 6-mm length of microlens was bonded to a copper mounting structure which was bolted to an arm attached to an X-Y-Z positioner. The diode-laser array and its driver circuit were attached to a mount which could be rotated until the linear array was co-parallel with the line focus of the cylindrical lens.

The divergence of the laser beam from the microlens-collimated array was determined from measurements of the far-field beam footprint dimensions. The measurements yielded $\theta_{\parallel} = 17.7^{\circ}$ and $\theta_{\perp} = 17$ *mrad*. The value of $\theta_{\perp}$ can be calculated from $\theta_{\perp}$ = junction width/focal length. This yields $\theta_{\perp} = 0.002/0.11 = 18$ *mrad*, which is in good agreement with the measured value. Vendor's data provides $\theta_{\parallel} = 19^{\circ}$ at the $1/e^2$ points.

A laser beam analyzer was used to generate the false-color image of the microlens-collimated beam shown in Figure 37. Due to the large value of $\theta_{\parallel}$, only a small section along the length of the beam could be displayed. The horizontal yellow (highest power) stripe indicates the center of the beam. Note that the vertical power profile is not Gaussian. The pronounced wings may indicate that the lens was not optimally aligned angularly with the diode array (only one axis of rotation was aligned)

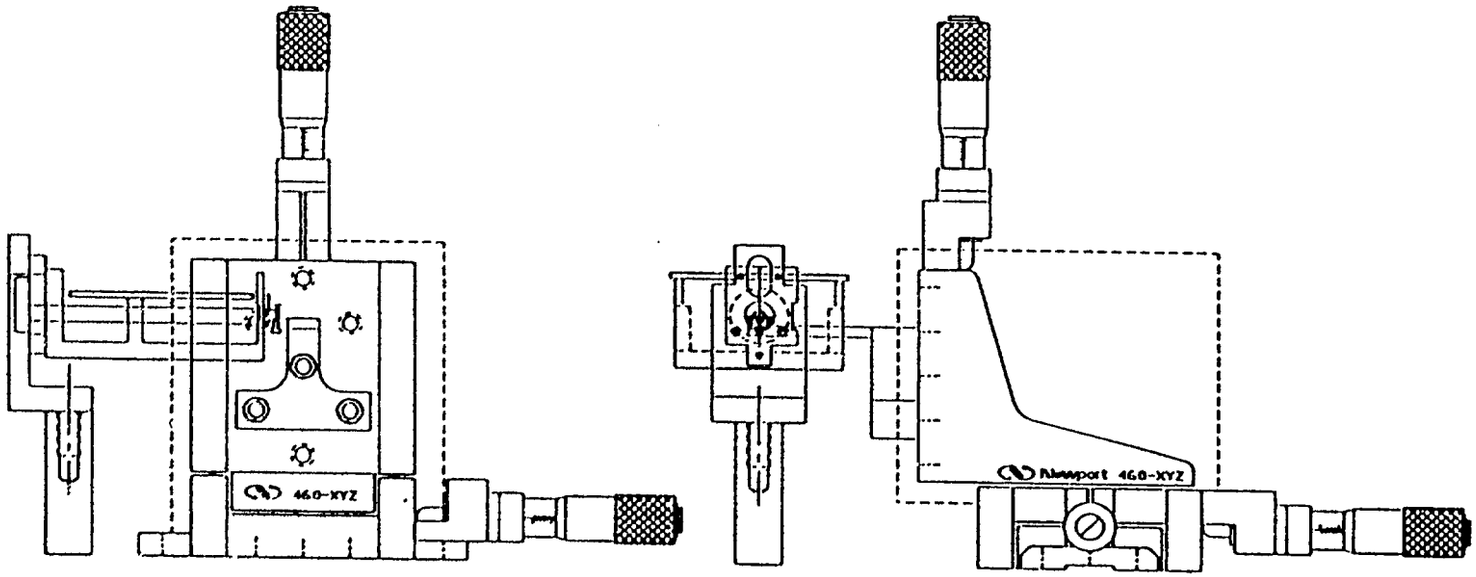

Figure 35. Microlens positioning setup

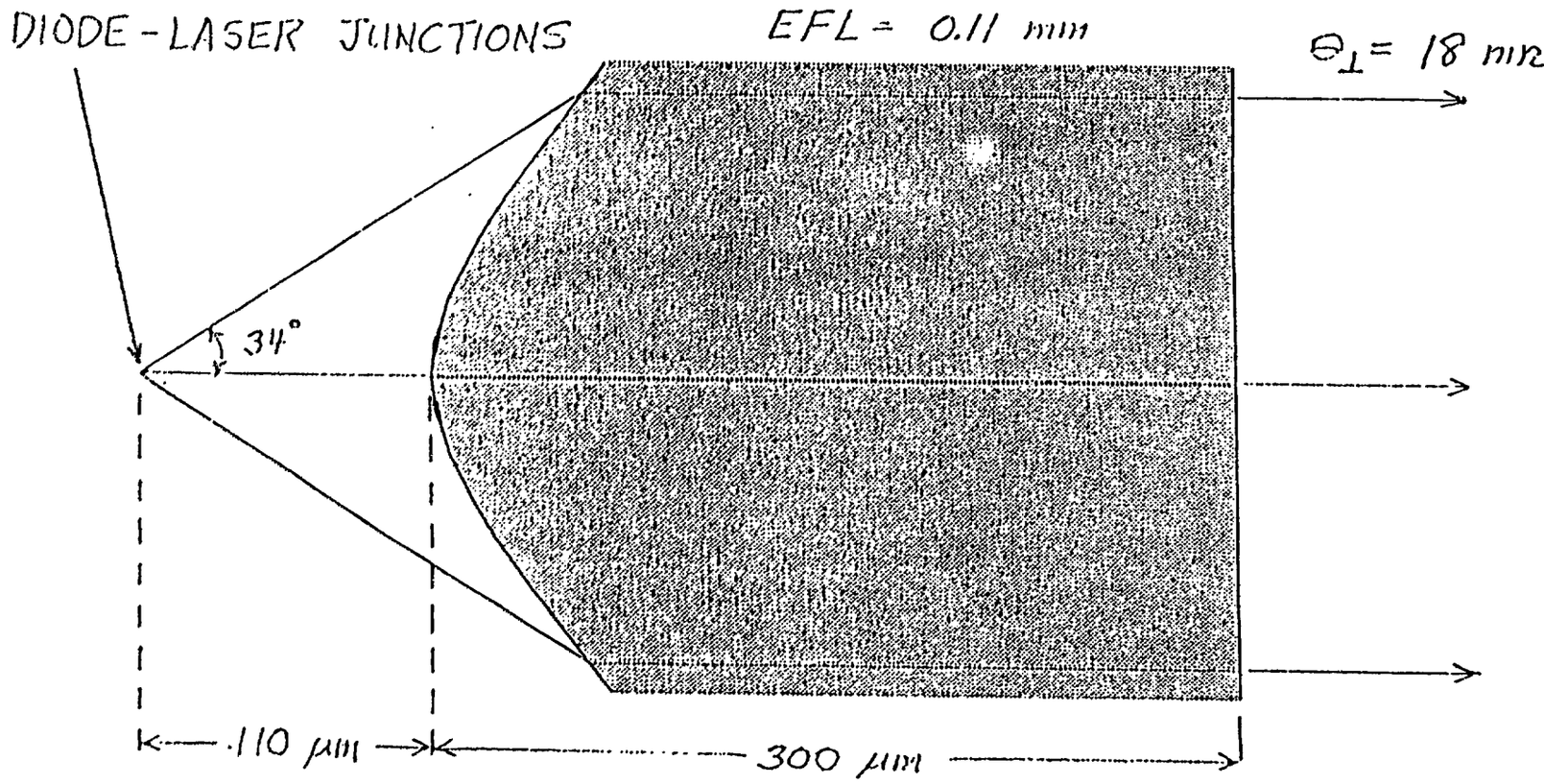

Figure 36. Cylindrical microlens collimator

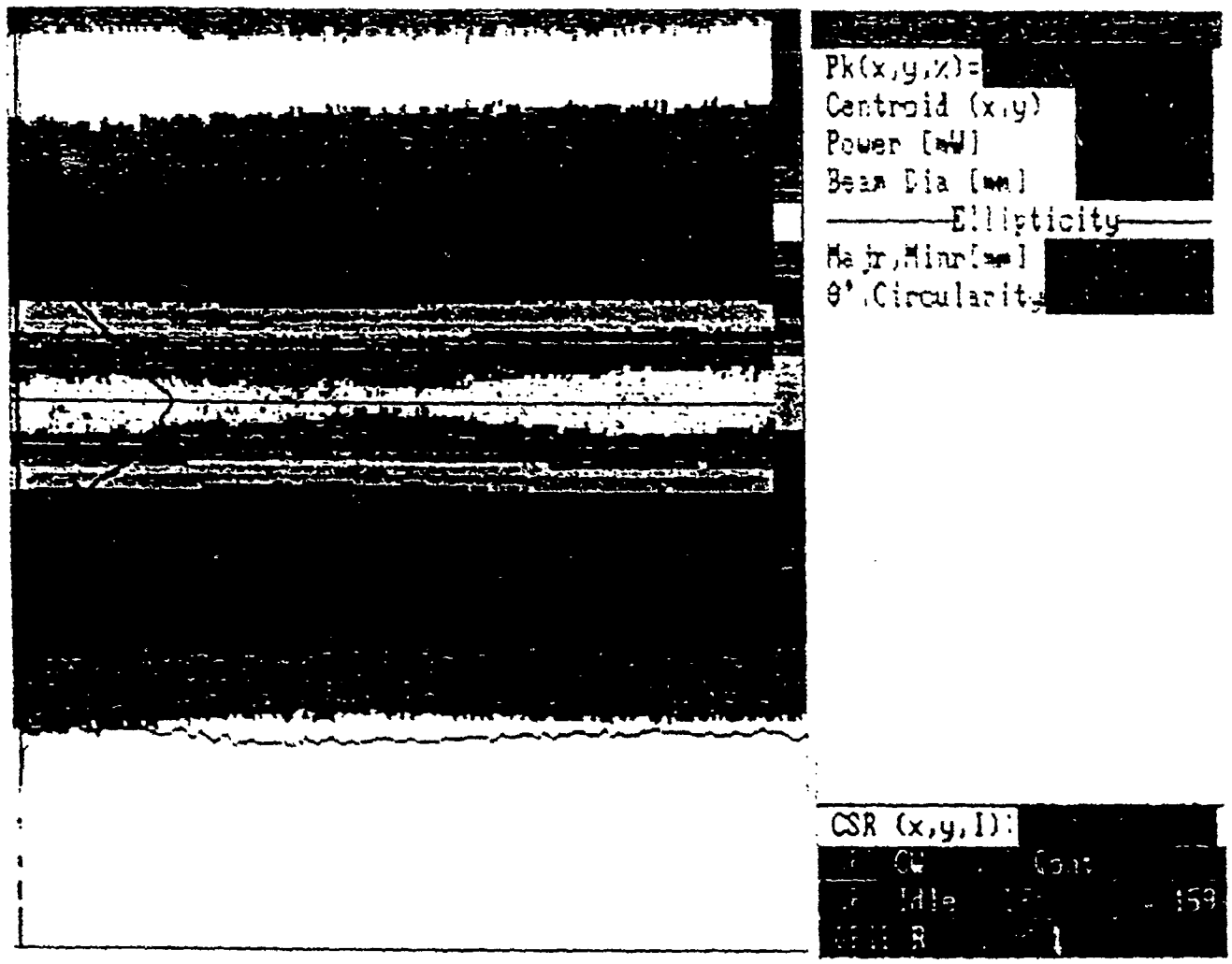

Figure 37. Microlens-collimated beam intensity contour and profile plots

After collimation was achieved, the lens was bonded in position by cementing the copper mounting structure to the diode laser heat sink with EC2216 epoxy. After curing overnight at room temperature, the beam profile shown in Figure 38 was obtained. This shows that a slight amount of defocusing occurred during curing. Disconnecting the copper mounting structure from the positioning arm resulted in further defocusing, as demonstrated by the beam profile shown in Figure 39.

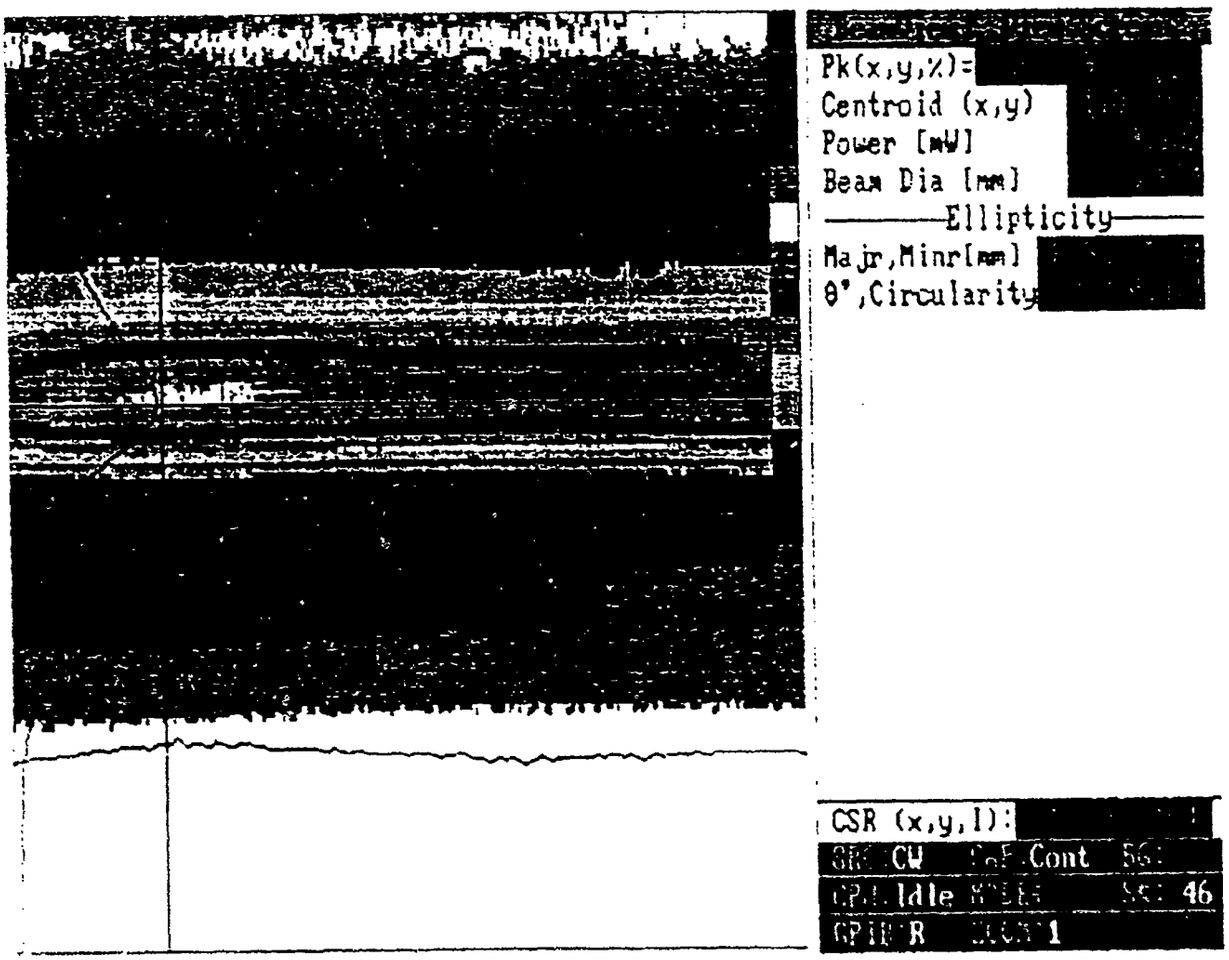

Figure 38. Beam intensity contour and profile plots after epoxy cure

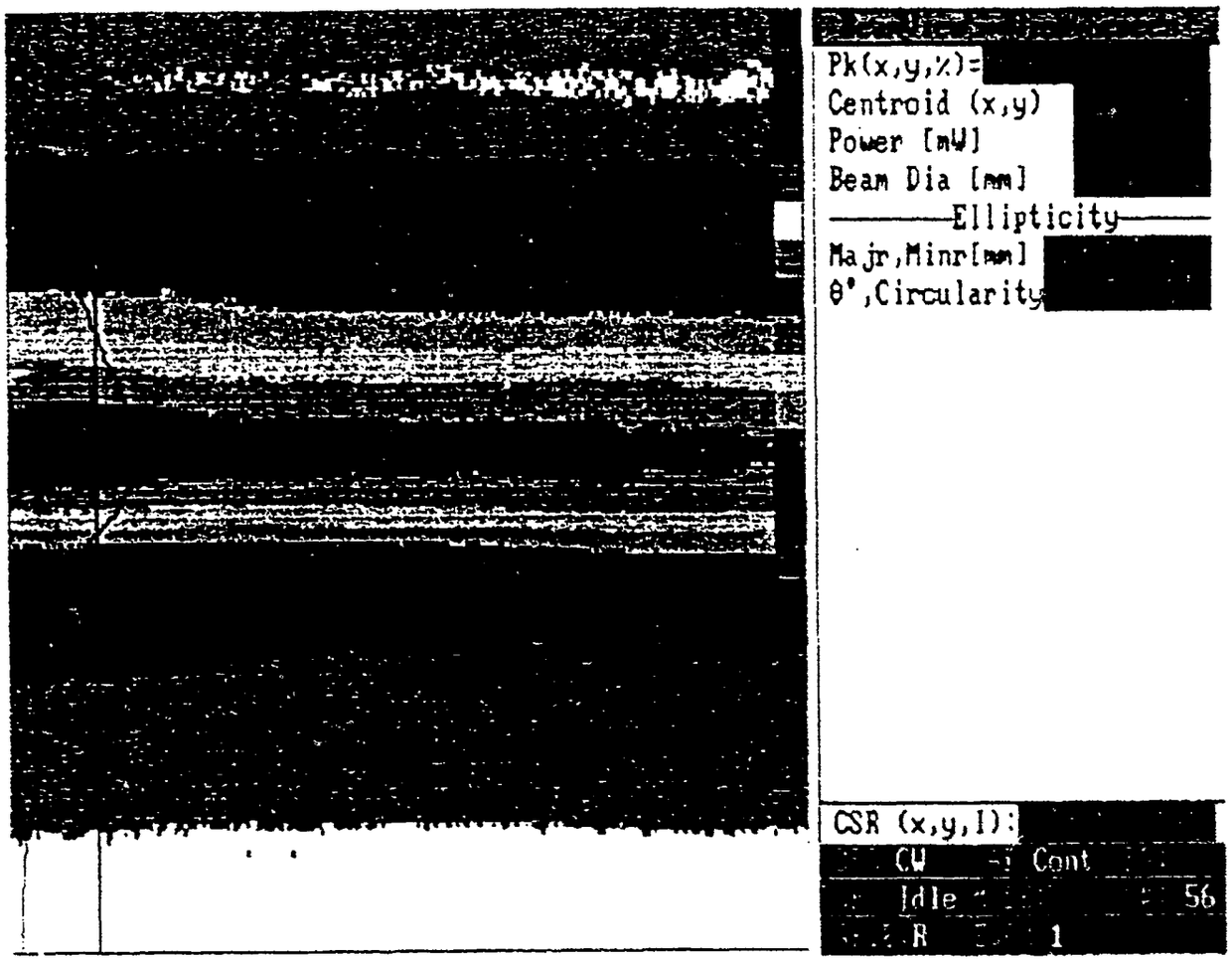

Figure 39. Beam intensity contour and profile plots after disconnecting lens positioner

SECTION IV
CONCLUSION

The process of developing an antireflection-coated diode laser resulted in two main conclusions. First, the best technique used to obtain uniform and reproducible SiO_x deposition was to evaporate pure Si under a controlled partial pressure of O_2. Second, the best technique used to determine the optimum coating thickness was to monitor the forward voltage drop across the diode lasers. The forward-voltage-drop technique consistently provided a well-defined peak at optimum coating thickness.

By using a narrow-band filter within an external cavity, the FWHM spectral bandwidth of a diode laser was reduced from 50 Angstroms to 2.5 Angstroms. Some of the drawbacks with the external-cavity technique were 1) reduction in laser output power, 2) critical alignment of cavity components required, and 3) sensitivity to environmental conditions (i.e. temperature changes and vibration). Test results showed that comparable spectral narrowing could be obtained with either AR-coated or standard-coated diode lasers. It remains to be determined whether additional spectral narrowing is possible with good AR coatings.

The line-narrowed range finder test results demonstrated that the maximum range capability of a line-narrowed system is 67 % greater than that of a conventional system using the same diode laser. The line-narrowed range finder was able to range to 484 ft with only 5.61 W of peak laser output power. When using the same laser but without the external cavity, we were able to range to 324 ft with 8.13 W of peak laser output power. The loss in laser output power resulting from the addition of the external cavity was $\simeq$ 30 %.

Before the line-narrowed range finder can be employed in the field, the following obstacles must be overcome: 1) special mounts must be manufactured that are temperature and vibration stable, 2) the output peak power must be greater than 30 W to be able to range to 1600 ft or greater, and 3) compact, efficient, spatial multiplexing of multiple diode lasers must be achieved. The development of a line-narrowed diode-laser transmitter that is temperature and vibration

stable with small beam divergence and high output power will make possible the fabrication of a cost-effective, long-range, diode-laser imaging radar system.

SECTION V
REFERENCES

1. J. Landreau and H. Nakajima, "In situ reflectivity monitoring of antireflection coatings on semiconductor laser facets through facet loss induced forward voltage changes," Appl. Phys. Lett., 56, 2376 (1990).

2. I.P. Kaminow, G. Eisenstein, and L.W. Stulz, "Measurement of the modal reflectivity of an antireflection coating on a superluminescent diode, " IEEE Quantum Electron, QE-19, 493 (1983).

DISTRIBUTION LIST
(WL-TR-93-7032)

DTIC/DDAC
Cameron Station
Alexandria VA 22304-6145
1

WL/MNOI (Scientific and Tech. Info. Facility)
203 W. Eglin Blvd., Ste 300
Eglin AFB FL 32542-6843
1

WL/MNGS
101 W. Eglin Blvd., Ste 209
Eglin AFB FL 32542-6810
4

AFDTC/PA
Eglin AFB FL 32542-6810
1